11-2017

Design and Prototyping of a Shape-changing Rigid-body Human Foot in Gait

Tanner N. Rolfe

Design and Prototyping of a Shape-changing Rigid-body Human Foot in Gait

Honors Thesis

Tanner N. Rolfe

Department: Mechanical Engineering

Advisors: Andrew P. Murray, Ph.D. and David H. Myszka, Ph.D.

November 2017

Design and Prototyping of a Shape-changing Rigid-body Human Foot in Gait

Honors Thesis

Tanner N. Rolfe

Department: Mechanical Engineering

Advisors: Andrew P. Murray, Ph.D. and David H. Myszka, Ph.D.

November 2017

Abstract

Traditional ankle-foot prostheses often replicate the physiological change in shape of the foot during gait via compliant mechanisms. In comparison, rigid-body feet tend to be simplistic and largely incapable of accurately representing the geometry of the human foot. Multi-segment rigid-body devices offer certain advantages over compliant mechanisms which may be desirable in the design of ankle-foot devices, including the ability to withstand greater loading, the ability to achieve more drastic shape-change, and the ability to be synthesized from their kinematics, allowing for realistic functionality without prior accounting of the complex internal kinetics of the foot. This work focuses on applying methodology of shape-changing kinematic synthesis to design and prototype a multi-segment rigid-body foot device capable of matching the dynamic change in shape of a human foot in gait. Included are discussions of an actuation strategy, mechanical design considerations, limitations, and potential prosthetic design implications of such a foot.

Acknowledgements

I'd like to thank the University of Dayton Honors Program, without whose support this project would not have been possible. I'd also like to thank the personnel of the University's Design of Innovative Machines Laboratory for their feedback during this project, especially Bingjue Li, Ethan Vantilburg, Cory Stuffelbeam, Ran Zhai, and Sean Conway for their technical contributions. My thanks as well to the following University of Dayton faculty for their knowledge and guidance: Dr. Allison Kinney, Dr. Joaquin Barrios, Dr. Timothy Reissman, and Jack O'Gorman. Special thanks to David Gravitt at Dayton Reliable Tool Mfg. Co. for his exceptional machining skills, and to my father, Nicholas Rolfe, for his assistance with data acquisition on the hottest day of summer. Lastly, I'd like to thank my advisors, Drs. Andrew Murray and David Myszka, for their mentorship and friendship throughout my undergraduate years.

UNIVERSITY of DAYTON

Table of Contents

1 INTRODUCTION

The foot is an incredibly intricate part of the human body, and plays an integral role in bipedal locomotion. The unique musculoskeletal structure of the foot provides basic stability, mechanical leverage, shock absorption, and balance during gait [1-3]. Traditional ankle-foot prostheses seek to replicate this same functionality for lower limb amputees, but in doing so, often oversimplify the geometry of the foot, limiting both the anatomical and biomechanical accuracy of these devices. Research driving modern prosthetic design has largely focused on increasing the energetic efficiency of prosthetic gait using roll-over geometry as a functionality metric, while comparatively little focus has been given to design approaches based on actual foot geometry.

This thesis describes the design process resulting in the creation of a shape-changing rigid-body foot mechanism capable of accurately portraying the dynamic change in shape of the foot during walking. The thesis document is organized as follows. The remainder of Chapter 1 will be dedicated to providing an overview of the roll-over shape in current prosthetic design and its limitations, as well as justification for the use of rigid-bodies to achieve shape-change in a foot device. Chapter 2 summarizes previous work developing a method of kinematic synthesis of shape-changing mechanisms. Chapter 3 describes the application of this method in the design and rapid prototyping of a shape-changing foot, while Chapter 4 discusses the potential benefits and limitations of this design, as well as recommendations for further development. Conclusions are presented in Chapter 5.

Throughout this document, various anatomical terms are used to describe features of the human foot. The reader is encouraged to consult Figure A1 in the Appendix, which provides a diagram of major bones and joints in the foot, as needed.

1.1 Roll-over Shape in Prosthetic Ankle-foot Design

The roll-over shape (ROS) consists of the set of coordinate points describing the location of the center of pressure on the plantar surface of the foot relative to the knee during the stance phase of gait [4]. When plotted on a shank-based coordinate plane (i.e. a 2D coordinate system defined by a vertical axis which passes through both the knee and

ankle joints), the points constituting the ROS align in an approximate rocker curve. Rocker curves have long been used in both computational and physical models of human locomotion [5-8]. Such models are appealing for their simplicity and relative accuracy [4], but the ROS is especially useful for clinical applications due to its invariance. Hansen and Childress have demonstrated that the ROS does not vary as a result of walking speed [9], carried torso weight [10], shoe heel height [11], or shoe rocker radius [12], and suggest that this invariance is due to a tendency for humans to actively adjust to level ground conditions to maintain the same roll-over geometry.

Data suggests that a ROS is unique to an individual [13], and is at least partially influenced by the individual's stature. Although the exact curvature of the foot has no significant effect on the rolling motion of walking [14], evidence exists suggesting that the arc length of the foot and its effective rocker radius have a noticeable effect on the rolling mechanics and energy costs of walking. Adamczyk and Kuo found that foot length influences the amount of work dissipated in foot collision with the ground during the rolling motion of step-to-step transition, while the foot arc radius determines the rate of advancement of the center of pressure and the resulting compensatory muscle forces [15, 16]. Empirical roll-over data from multiple studies [9, 15, 16] has shown to closely match modeling predictions of a metabolically optimal rocker radius approximately equal to 30% of leg length [6]. This proportion also closely matches the average ratio of human foot length to leg length [9, 15-17]. The recurrence of these proportions throughout the literature suggests the existence of an ideal foot geometry that would produce an invariant, energetically optimal ROS.

For the reasons listed above, the ROS has been adopted by many prosthetists as an ideal metric of walking functionality, leading to the design goal of matching the ROS of a natural, unimpaired foot [4, 18, 19]. This design goal was the inspiration for a relatively novel prosthesis developed in 2004 by researchers at the Northwestern University Prosthetics-Orthotics Center called the 'Shape&Roll' (S&R) foot [20]. Designed as an alternative to cheaply manufactured but cumbersome conventional foot prostheses such as the SACH (solid-ankle cushion-heel) foot and various SACH derivatives commonly used in low income regions [20-22], the S&R foot consists of a flexible, molded

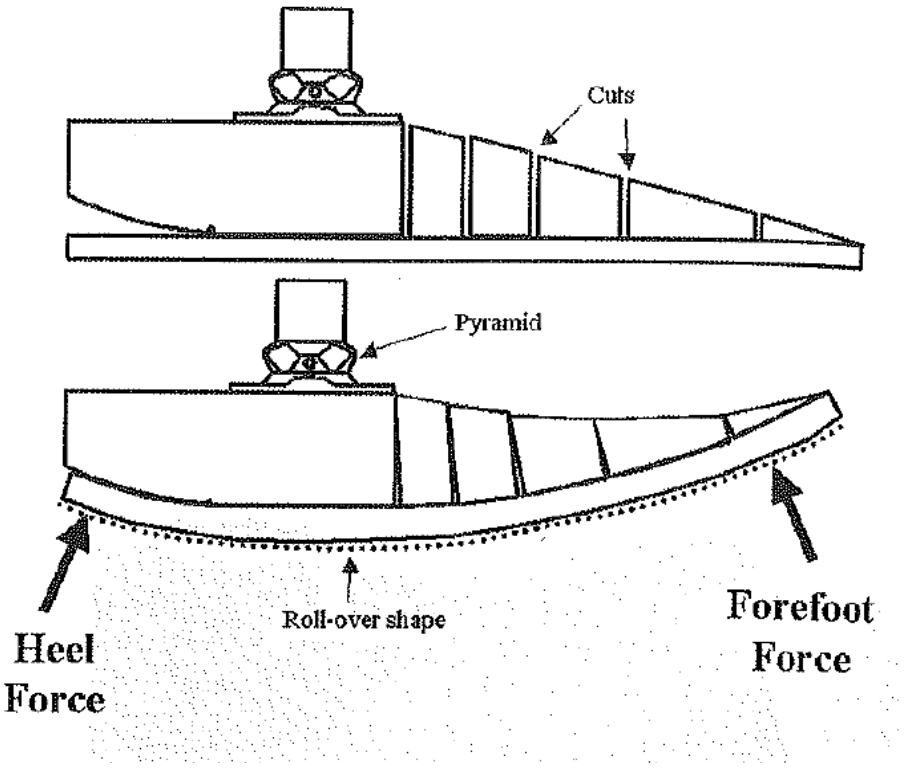

Figure 1. *Sagittal plane diagrams of the core of a S&R prosthesis. Image adapted from Ref. [20].*

copolymer core (shown in Figure 1) with a series of cuts spaced along a tapered forefoot ridge. The width and spacing of the cuts is determined by measurement of the user's stature. The cuts are designed to facilitate flexion of the thinner, wider sole portion of the core in response to ground reaction forces (GRFs), while prohibiting flexion beyond the degree specified by the ROS. Flexion of the hindfoot is limited by a contoured cutout above the sole at the heel. The cutout additionally provides space for a compressible wedge to be inserted at the heel to provide shock absorption in a manner similar to conventional SACH prostheses.

Initial comparative roll-over testing of the S&R foot against traditional prosthetic designs (Figure 2) including a SACH foot and an Össur Flex-walk foot (a type of energy-storage-and-return, or ESAR, foot more commonly used in industrialized nations) showed that the S&R foot produced a consistent ROS that matched the biological ROS with an accuracy comparable to or greater than the Flex-walk foot, and far more accurately than the SACH foot [20]. Field test participants displayed a greater preference for the S&R

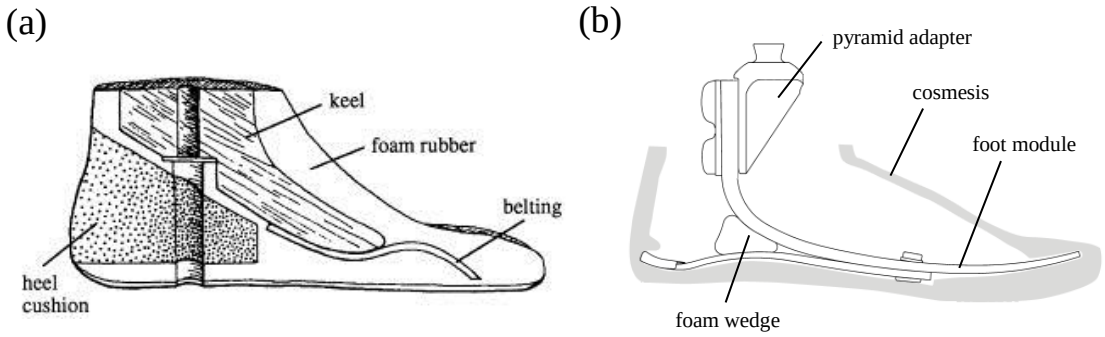

Figure 2. *Typical constructions of (a) a conventional SACH foot and (b) an Össur Flex-Foot Assure, a common example of an ESAR foot. Images adapted from Refs. [23] and [24], respectively.*

foot, stating that gait felt more natural as a result of the closer adherence to the biological ROS [21]. In addition to the cuts which facilitate flexion of the core into a rocker shape, the ability of the S&R to more closely replicate the natural ROS is aided by the extended arc length of the core, which closely matches the optimal foot proportions propounded by Adamczyk and Kuo and others [9, 15-17]. In comparison, the SACH foot and its derivatives have a short effective arc length, as the rigid keel which provides the rolling mechanical leverage during gait does not extend the full length of the foot. As a result, roll-over analysis of conventional feet shows a pronounced "drop-off" of the ROS during the latter stages of stance due to a lack of forefoot support [22, 25].

While the success of the S&R foot provides some validation for the use of the ROS as a primary design metric for ankle-foot prostheses, there are limitations associated with the ROS. Curtze et al. note that for prosthetic users, there exists an inherent asymmetry between the ROS of a prosthetic foot and the nondisabled foot due to the inescapable physical and geometric differences between the two, as opposed to nondisabled walking, which is reasonably symmetric [13]. As a result, there is a natural tendency to favor the nondisabled foot, which can lead to further asymmetry and gait complications as a result of overcompensation. Additionally, Olesnavage and Winter demonstrated that it is possible for a prosthetic foot to match the physiological ROS, but exhibit vastly different lower leg kinematics in response to the same GRFs [26], suggesting that the ROS alone is unable to fully characterize the motion of the ankle-foot system. Klodd and Hansen also found through experimentation using S&R feet with different effective rocker radii that

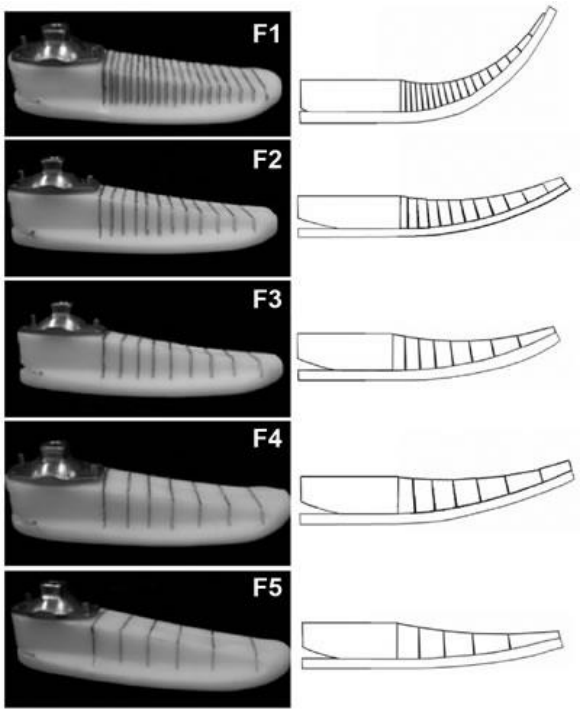

Figure 3. *Five S&R variants used to test the effects of prosthetic forefoot flexibility on gait. The ROS produced by each is determined by the width and spacing of the cuts placed in the forefoot region of each variant. Image adapted from Ref. [25].*

feet with ROSs of significantly smaller radii than the optimal proportions suggested by Adamczyk and Kuo and others (the F1 variant shown in Figure 3) exhibit the same drop-off effect seen in SACH feet as a consequence of the decreased stiffness in the forefoot region required to achieve the tighter rocker radii [25]. This implies that for individuals with a disproportionate foot size, concessions in the design of a prostheses required to match the ROS may have undesirable consequences on comfort and energy use [16].

One of the potential pitfalls of using the ROS as a catch-all metric of functional design is the tendency to sacrifice foot geometries that do not affect the ROS but that nonetheless provide an important role in gait, such as the geometry of the plantar surface in contact with the ground. The curvatures of the plantar arches of the foot have a large influence on balance, stability, and the distribution of weight during gait [1, 2], and it is well documented that the plantar surface deforms when subjected to varying loads during walking [27, 28]. Conventional foot designs including the S&R foot have relegated this geometry to cosmeses, where it serves as more of a cosmetic feature (as the name would imply) than a functional one. The mechanical leverage required for forward propulsion (which ultimately relies on the GRFs and their distribution across the bottom surface of the foot), however, is dependent on the shape and stiffness of the core. For this reason, more current ESAR foot designs have attempted to incorporate plantar curvature into the core of the prostheses, and have in some designs eliminated the cosmesis entirely [29]. The cores of these feet are typically a single body made of a compliant composite material (such as carbon fiber) capable of relatively small deformations that behaves

much like a leaf spring, which provides the primary mechanism for energy storage and release, reducing the amount of work required of the user [29, 30]. Because of the varying stiffness requirements for different regions of the foot, however, a single body core is limited in the deformation it is able to achieve. While it has been shown that ESAR feet are capable of matching a physiological ROS with relative accuracy comparable to the S&R foot [20], focus groups consisting of both ESAR and conventional foot users consistently identify a general lack of mobility and frequent loss of balance due to limited range of motion as one of the most prevalent challenges encountered by lower limb amputees [31, 32].

The limitations associated with the ROS, as well as the restricted motion of current prosthetic designs may be addressed by closer replication of the change in plantar shape of the foot during walking. A prosthesis capable of achieving realistic shape-change may help address the asymmetry in gait noted by Curtze et al. [13], as an adherence to actual foot geometry will theoretically provide a physiologically accurate ROS while maintaining the curvature required for proper balance and weight distribution, potentially increasing user confidence in the disabled limb and reducing compensation with the nondisabled limb. Furthermore, a prostheses able to deform in the same manner as the biological foot would offer more versatility than current designs, increasing user comfort and mobility while reducing lifestyle restrictions imposed by the difficulty of performing basic occupational tasks.

1.2 Shape-change Mechanisms & Potential Advantages of Rigid-body Shape-change in Prosthetic Design

Shape-change refers to the ability of a mechanical system to dynamically alter its physical geometry to achieve a specific function or to enhance performance. Shape-change can be achieved through the use of a chain of rigid-bodies, compliant materials, or a combination of both. Conventional prosthetic feet, like the SACH foot, typically consist of both a rigid keel and a compliant cosmesis, but the shift toward more energetically efficient ESAR feet during recent decades has led to a proclivity toward the use of compliant composite materials to achieve shape-change due to their generally higher

elasticity. There is indeed an elastic character to the physiology of the foot: the elasticity of the skin and muscular tissue in the foot helps provide shock absorption during gait, storing energy through elastic deformation and releasing the stored energy to aid in forward propulsion during toe-off. Ruina et al. have demonstrated that the metabolic cost of gait is minimized for walking modeled as a sequence of pseudo-elastic collisions, while a comparatively large amount of energy is lost through collisions in rigid-body locomotion [14]. In general, compliant materials also have a high surface accuracy and can thus achieve smooth contours, which resemble the curved structure of the foot and are thus cosmetically appealing.

While compliant materials can offer more elasticity than rigid-bodies, the high-strength composite materials generally used in the manufacture of prosthetic feet are still an emerging technology, and are often expensive as a result. The kinematics and kinetics of compliant materials can also be challenging to characterize mathematically, whereas analysis of rigid-body systems is comparatively simple. Furthermore, advances in additive manufacturing have allowed rigid materials to take on more exotic and complex geometries than possible with traditional machining processes. As a result, rigid materials can be more easily shaped to match irregular contours, lending them a greater competitive edge against compliant materials for precision applications.

There are multiple advantages offered by rigid-bodies that may be beneficial in the design of a prosthetic foot. Due to their inelastic character, rigid materials often have a higher yield strength than more ductile compliant materials, making them less susceptible to static failure as a result of overloading. Prosthetic users have noted poor material strength and durability as a prevalent problem with current prostheses, with multiple focus group participants identifying frequent failure in response to relatively small increases in carry weight [31]. Due to their stiffness, rigid materials also offer greater mechanical leverage. While some elasticity is required to absorb energy and later release energy that would otherwise be lost in collision during initial heel strike, sufficient structural rigidity is also required to provide enough mechanical leverage to facilitate forward propulsion. While careful balancing of a rigid-body foot would be required to avoid premature advancement of the center of pressure during gait [16], a greater

mechanical leverage would potentially amplify the component of forward momentum imparted by horizontal GRFs, reducing the metabolic contribution to propulsion. In addition, rigid-body mechanisms are capable of achieving comparatively large displacements, resulting in more drastic shape-change. A larger range of motion would allow a foot device to reach a greater number of configurations, potentially increasing the utility and variety of postures that can be achieved. Such versatility may go a long way in addressing the lack of mobility and restriction of freedoms experienced by many prosthetic users [31, 32].

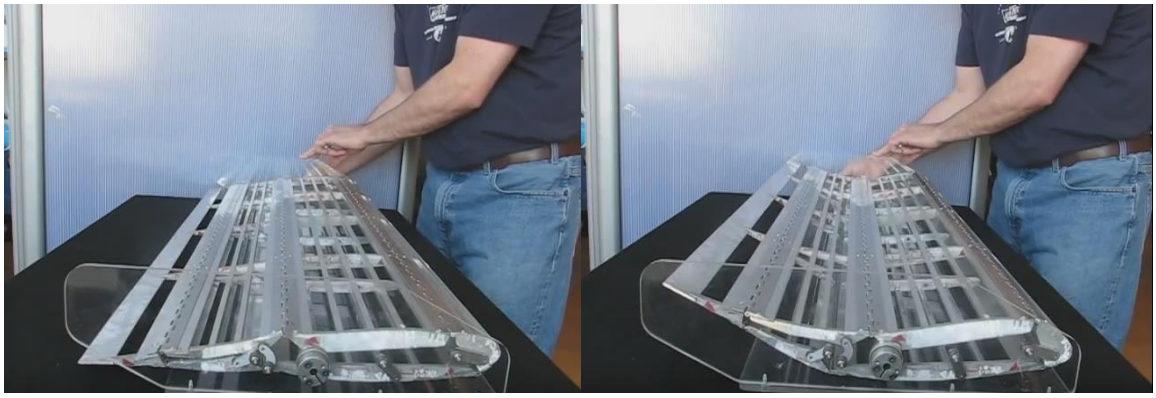

Figure 4. *A prototype of an automobile spoiler frame in two different configurations, demonstrating shape-change via an array of rigid-body chains. Image adapted from [33].*

Unlike compliant shape-change mechanisms, multiple rigid-bodies arranged in a chain are required to achieve a change in geometry. Rigid-body chains (such as the ones in the array shown in Figure 4) are composed of inflexible links connected by mechanical joints. For planar mechanisms, these joints can include: revolute joints, which allow one link to rotate relative to the next; prismatic joints, which allow a link to translate along a path dictated by the geometry of the joint; and fixed connections, or fused joints, which keep one link fixed relative to the next, effectively "fusing" multiple links into a single member. Each link and joint provides a degree of freedom (DOF), an independent parameter defining the mobility of the chain. The mobility of nonstructural planar kinematic chains can be expressed using the Gruebler equation:

$$D = 3(n-1) - 2J_1 - J_2 \tag{1}$$

where D is the total DOF of the chain, n is the number of links in the chain, J_1 is the

number of 1 DOF joints (such as revolute or prismatic joints), and J_2 is the number of higher-order joints (such as cam or gear joints) [34]. It is highly desirable to keep the number of DOF a system has low in order to reduce the number of inputs to the system required to achieve the desired configurations. This is typically done by arranging links in dyads, thus tying the motion of multiple links to a single actuator.

The motion of multiple DOF rigid-body linkages is difficult and in many cases impossible to achieve passively. The requirement of active elements, ample space to place said elements, and a power source presents a large obstacle for prosthetic applications of such systems. Conventional feet and traditional ESAR feet move passively during walking. Their motion is entirely dependent upon the changes in position of the leg and the corresponding GRFs during stance. While single segment compliant bodies are conducive to the passivity of the foot in such a model of walking, they bear little physiological accuracy. The foot is not a singular body; it is composed of multiple joints, muscles, and ligaments that expand and contract to control positioning of the foot. The limited effectiveness of conventional and passive ESAR feet has in recent years led to the development of more robust 'bionic' feet; that is, feet containing one or more active elements, often neuroelectrically controlled [29]. While bionics is still an emerging technology, the promising energetic efficiency of bionic prostheses has helped establish a precedent for the inclusion of active elements in prosthetic design, an almost certain requirement of any multi-segment rigid-body foot.

Perhaps the most significant benefit offered by a multi-segment rigid-body foot is the ability of a chain of rigid links to be synthesized directly from the kinematics, achieving realistic functionality without the need for a priori knowledge of the complex internal kinetics of the human foot, which are often difficult to characterize. Thus, based upon positional data, it is possible to design a rigid-body mechanism that approximates the motion and change in shape of an actual foot. The procedure originally introduced by Murray, Schmiedeler, and Korte [35], and later expanded upon by Persinger [36] and Shamsudin [37] provides a method of synthesis for shape-changing rigid-body mechanisms based on positional inputs referred to as design profiles that describe the set of shapes for which a configurational match is desired. From positional configurations of

a shape-changing mechanism, other useful characteristics of the motion represented by design profiles, such as velocities and accelerations, can be derived. An understanding of the kinematics of certain points on the foot is vital to effectively model human gait (e.g. the trajectory and rate of advancement of the center of pressure is required to characterize the ROS). To the extent of the author's knowledge, the design of a rigid-body ankle-foot prosthesis based primarily on the structural geometry of the foot and its change during gait as characterized by the kinematics has never been attempted.

As a final statement on the applicability of rigid-body synthesis to prosthetic design, it is important to note that the best design solution may not be attainable by the independent usage of rigid-body or complaint mechanisms of shape-change, but rather by a combination of the advantages provided by both. The two are not mutually exclusive, and while this project primarily focuses on the use of rigid-body synthesis techniques to produce a viable foot device (as there seems to be a dearth of exclusively rigid-body prosthetics in the literature), it is possible that such a device can only exist with the inclusion of compliant components. The author encourages future work stemming from this project to explore the potential applicability of both rigid and compliant additions to the design developed in the following chapters.

2 SHAPE-CHANGING RIGID-BODY SYNTHESIS

The following section provides a summary of the methodology for synthesis of a shape-changing chain of rigid links as described in Refs. [35-37]. Practical devices synthesized using this methodology have thus far largely been limited to non-biological applications, such as morphing aircraft wings [38], automobile spoilers [33], and polymer extrusion dies [39]. It has previously been demonstrated, however, that the technique can be applied successfully to a variety of morphometric problems with biologically generated inputs [40].

The synthesis process originates with a set of p curves called design profiles that describe the shapes for which a match is desired. Design profiles can be open or closed and can have fixed or variable endpoint positions. The design profiles generated in this work are

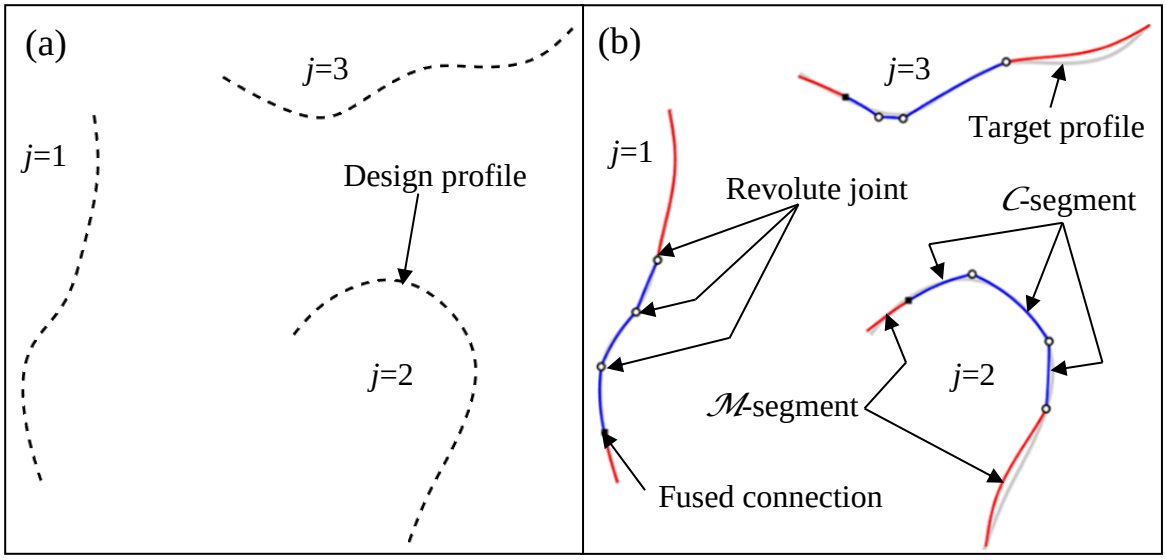

Figure 5. *An example set of (a) open design profiles and (b) a corresponding set of target profiles approximated by a single chain of links.*

open, with the curves beginning at a point near the tip of the hallux (first toe) to a point at the base of the heel. Figure 5a provides an example of three different open design profiles. Design profiles are approximated as target profiles, piecewise linear curves of virtually equal piece length. Target profiles are generated by spacing N_j points (where j is the profile number) equidistantly along the design profile. Each point (with the exception of the first and last endpoints) describes the location of the shared endpoint between two contiguous linear pieces, meaning that a design profile j approximated using N_j points will have a corresponding j^{th} target profile consisting of N_j - 1 pieces. The arc length of the j^{th} target profile is thus quantified by the number of pieces it contains. For example, the target profiles j=1, j=2, and j=3 in Figure 5b have arc lengths of 1012, 1152, and 1000 pieces, respectively, based on a specified minimum profile length of 1000 pieces. The average piece length is 0.0522. The greater the number of pieces in each target profile, the better the approximation of the corresponding design profile, and the smaller the average piece length. While the minimum number of pieces used to generate each target profile is determined at the discretion of the designer, a smaller number of pieces will require less time to compute.

Following generation of the target profiles, the rigid-body chain approximating these profiles is specified through an operation referred to as segmentation. The desired chain is defined by a pair of design vectors that describe the types of segments (rigid links)

constituting the chain and the types of connections (joints) between each segment. These vectors are the segment type vector **V** and the connection type vector **W**, respectively. The segment type vector **V** is comprised of q elements, where q is the desired number of segments. Each element in the vector is one of two segment types, $\mathcal{M}$ or C. $\mathcal{M}$-segments have a fixed shape approximating a portion of each target profile containing the same number of pieces in all profiles. Thus, an $\mathcal{M}$-segment may be embodied by a single rigid link in a physical chain. C-segments have a constant curvature, but a variable arc length, thus approximating a different number of pieces for each target profile. Mechanically, a C-segment may be embodied by a pair of links connected by a prismatic joint which slides along the path of curvature, thus allowing the segment to expand or contract (this construction is typically referred to as a revolute-prismatic-revolute , or RPR, chain). While a set of target profiles with similar arc length can be approximated by a segment type vector consisting of only $\mathcal{M}$-segments, profiles with significant difference in arc length require at least one C-segment in the segment type vector in order for the chain to achieve an adequate match [37]. The connection type vector **W** contains q - 1 elements of type $\mathcal{R}$ or type $\mathcal{F}$. $\mathcal{R}$ type connections represent a revolute joint connecting two adjacent segments, allowing one segment to rotationally position itself at a unique angle relative to the other segment for each target profile. $\mathcal{F}$ type connections represent a fused connection between two adjacent segments, joining the segments at the same fixed angle for all profiles. The segment and connection type vectors for the example chain shown in Fig. 5b are **V** = [$\mathcal{M}$ C C C $\mathcal{M}$] and **W** = [$\mathcal{F}$ $\mathcal{R}$ $\mathcal{R}$ $\mathcal{R}$], respectively.

After specifying **V** and **W** vectors, an initial population of p x q segment matrices is randomly generated. Each element m^e_j of a segment matrix (SM) describes the number of pieces approximated by the e^{th} segment of the segment type vector for the j^{th} profile. If the e^{th} element of the segment type vector is specified as an $\mathcal{M}$-segment, the shape of the segment is defined by the average shape of the corresponding portions of each target profile. If the e^{th} element of the segment type vector is specified as a C-segment, the curvature of the segment is defined by the average curvature of the points constituting the corresponding portions of each target profile, with the length of each piece constituting the segment equal to the average length of each piece in the corresponding portions of the

target profiles. The generated segments are then positioned along each target profile so as to minimize the point-to-point matching error associated with each profile.

The segments are joined according to the connection type vector. Segments connected by an $\mathcal{F}$ type connection are joined first by aligning the endpoints of the connecting segments, and fusing the segments together at a fixed angle equal to the average angle between the segments for each target profile. $\mathcal{R}$ type connections are joined in a similar manner, but instead of being joined at the same fixed angle for all profiles, segments are joined at the unique angle resulting in the lowest matching error for each profile. Note that the joining of $\mathcal{R}$ type connections need not be performed at this stage of the synthesis process. It is advisable to join segments connected by $\mathcal{R}$ type connections after SMs have been optimized, as doing so beforehand has been demonstrated to significantly increase computation time without significantly affecting post-optimization results [40].

After segments have been joined, all segments are repositioned along each profile to reevaluate the matching error. The matching error associated with a SM is defined by a corresponding p x q error matrix EM, where each element E^e_j describes the maximum matching error of the e^{th} segment of the segment type vector for the j^{th} profile. SMs are then optimized using an iterative, gradient-based method. In each step of iteration, segments are regenerated and rejoined based on the segment type and connection type vectors and the SM generated in the previous step, which yields a new EM with each iteration. The number of pieces constituting each segment is then adjusted to reduce the matching error based on the EM generated in the previous step. An optimal SM is achieved once no decrease in the overall matching error (defined as the average value of the corresponding EM) occurs after ten steps of iteration. Note that, typically, only the initial SM or SMs which produce the lowest average matching error are optimized in order to increase computational efficiency. Segments connected by $\mathcal{R}$ -type connections are now joined if they have not already been so prior to optimization.

As an example, the optimized SM describing the target profiles in Fig. 5b with the previously specified design vectors is:

$$SM = \begin{bmatrix} 147 & 180 & 196 & 108 & 381 \\ 147 & 165 & 312 & 147 & 381 \\ 147 & 57 & 123 & 292 & 381 \end{bmatrix}$$

Note that all entries in the 1st and 5th columns of the above SM are identical. These columns correspond to the $\mathcal{M}$-segments in the segment type vector, which contain an equal number of pieces for each profile. The final rigid-body chain is shown in Fig. 5b. Also note that the sum of the values in each row of the SM is equal to the total number of pieces in the corresponding profile (1012, 1152, and 1000 as previously stated). The corresponding EM is:

$$EM = \begin{bmatrix} 0.0236 & 0.0685 & 0.4790 & 0.4790 & 0.4806 \\ 0.6804 & 0.6017 & 1.3143 & 0.5928 & 0.7287 \\ 0.3064 & 0.4384 & 0.4871 & 0.4871 & 1.3280 \end{bmatrix}$$

which has an average point-to-point matching error of 0.5664.

A more in-depth development of the synthesis process described above can be found in Ref. [37]. All relevant calculations in this work were performed using a suite of routines in MATLAB developed and compiled by the University of Dayton's Design of Innovative Machines Laboratory (DIMLab). The suite allows the designer to input an existing set of design profiles, or create a new set, and generate an initial population of SMs from the resulting target profiles based on a specified segment type and connection type vector. Use of this suite allows for rapid calculation of optimal SMs, allowing the designer to more efficiently explore different combinations of design vectors.

3 DESIGN OF A SHAPE-CHANGING, RIGID-BODY FOOT

The following sections detail the design process resulting in a multi-segment, shape-changing, rigid-body prototype of a mechanical foot capable of matching the change in profile of the foot during walking. It should be emphasized that the design detailed in the following sections is not itself a prosthetic device. While the foot's design was heavily inspired by principles of prosthetic design, the primary design objective of this foot was

to demonstrate realistic shape-change based on methods of kinematic synthesis. As a result, emphasis was placed in many regards on form more so than function. Recommended future work on this project is guided toward adapting the design for biomechanical use and introducing additional functionality to increase its viability as a prosthetic device (see Section 4.3). Novel prosthetic design implications resulting from this work are discussed in Section 4.2. Section 3.1 outlines the procedure used to generate geometric profile data from biological gait. Section 3.2 details the kinematic synthesis of the chain of rigid-links constituting the foot. Section 3.3 describes the construction of a solid model of the foot, while Section 3.4 justifies the design choices made in the modeling process. Progress to date on development of an actuation strategy is presented in Section 3.5. Section 3.6 introduces the physical prototype of the foot and discusses its current state, as well as suggested improvements.

3.1 Generation of Design Profiles

In this work, 2D profiles derived from digital imagery of a human foot walking on level ground were used to generate design profiles. Ideally, profiles of the entire plantar surface of the foot would be used to best characterize foot geometry, as the topography of the bottom of the foot varies transversally. Traditional methods of obtaining digitized, 3D profiles of the plantar surface such as 3D scanning or pedobarographic pressure mapping are typically only capable of capturing one profile of the foot in a static position such as midstance. While methods of capturing multiple plantar profiles during dynamic activity such as walking exist [41-44], these methods were not employed in this work due to a lack of access to required technology. Additionally, the methods of kinematic synthesis described in Chapter 2 have thus far only been extended to planar mechanisms. While an array of planar rigid-body chains could in theory be used to recreate the transversal variance of the plantar profile, the resulting DOF and the complexity of the required synchronization between chains would result in a highly unwieldy and impractical foot. For these reasons, only 2D profiles taken from the medial view of the foot were used as design profiles.

The foot of a healthy, young adult male with no gait abnormalities was used to generate a set of design profiles from digital photographic images taken at 33 millisecond intervals

from the initiation of the stance phase of gait (initial heel strike) to the termination of the stance phase (toe-off). The subject walked on a level, elevated platform in front of a camera placed approximately 8 feet away on a stand level with the platform. Prior to capturing the images, the subject was asked to stand upright, and the inside medial edge of the subject's right foot was marked with a dashed ink line where it contacted the ground. An additional ink marking was placed at the ankle for reference. As the subject walked, the ink line would deform as the foot transitioned through the various stages of stance, providing an approximate contour of the bottom of the foot. Starting at the instance of initial heel strike, a total of 26 images were taken over a duration of 834 milliseconds before the foot lifted completely from the ground.

In order to reduce the total number of design profiles and thus reduce potential error during synthesis of the rigid-body chain, 16 non-sequential images containing insignificant change in profile from the previous image were discarded. The remaining 10 images, consisting of at least one image taken at each of the major stance stages, were used to generate 10 corresponding design profiles (Figure 6). The design profiles identified from these images were digitized using a MATLAB script allowing the user to draw a curve overtop an imported image. To draw the curve, the user would specify a set of points located on a coordinate plane originating at a reference pixel common to each image. A natural cubic spline was then fit to the set of user-specified points, interpolating the curvature from one point to the next. In order to obtain an accurate profile curve, points lying along the ink line marker were chosen to define the spline.

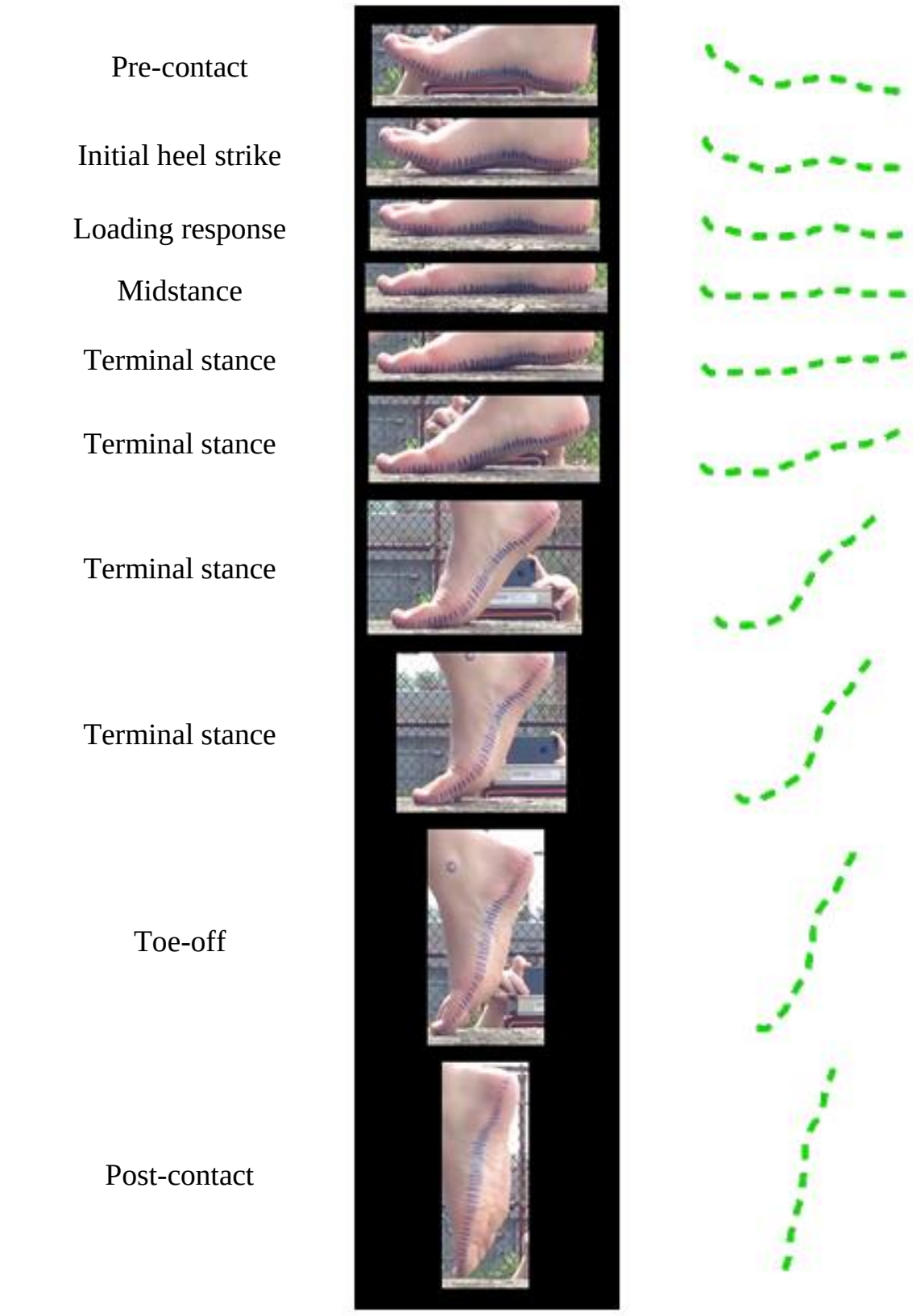

Figure 6. *Images taken of a foot during the stance phase of gait (middle) used to generate design profiles (right). Each image corresponds to a different stage of stance (left).*

3.2 Segmentation and Chain Generation

Before employing the kinematic synthesis methods outlined in Chapter 2, the 10 design profiles were carefully examined in order to guide the selection of user-specified parameters. Because of the relatively large potential for error associated with visual approximation of the profile of the edge of the foot in contact with the ground, as well as the large number of design profiles to match, a minimum profile length of 1000 pieces was specified for the 10 design profiles. While selection of a greater minimum limit would result in more accurate target profiles, the increase in computation time required for a comparatively small increase in the accuracy of an already approximate set of data yields diminishing returns. In addition, it was desirable to keep the length of the design vector small in order to produce a chain with a feasibly controllable number of rigid segments. Through repeated calculation, it was observed that at six or more segments, optimal SMs contained at least one element in each row of significantly lesser value than the other elements in the same row, resulting in impractically small segment sizes. Too few segments, however, resulted in poor matching of target profiles. A total number of five segments was chosen in order to balance segment size with match accuracy. It should be noted that because the optimization process relies on an initial population of randomly generated SMs, it may be possible to generate a chain of comparable accuracy containing a lower number of segments. However, given the myriad possible combinations of segment and connection type vectors, this is virtually impossible to predict without extensive trial and error.

Given the tight manufacturing tolerances and the generous amount of space required to implement a curved, sliding prismatic joint, it was desirable to specify a segment type vector **V** with as few *C*-segments as possible, noting again that at least one *C*-segment is required to match the shape of profiles with significantly different arc lengths. For this reason, careful consideration of the design profiles was necessary in order to choose a segment type vector that would result in an appropriate placement of the *C*-segment. It was observed that the largest difference in curvature between the profiles corresponded to a portion of each profile representing the ball of the foot, where the metatarsophalangeal joints are located. In comparison, the change in geometry of the portions of the profiles

corresponding to the hallux and the heel was relatively minor. Therefore, logical placement of the $\mathcal{C}$-segment was assigned to one of the three middle elements of the segment type vector. In determining the connection type vector **W**, it was desirable to use $\mathcal{R}$-type connections (revolute joints) in order to facilitate a greater degree of shape-change. While the use of $\mathcal{F}$-type connections would serve to reduce the required number of links by fusing two segments together at a fixed angle (effectively creating a single segment), the matching error associated with this combined segment would likely increase, given the inconsistencies in the curvatures of corresponding portions of the profiles resulting from the unavoidable positional error prompted by visual identification of the design profile splines.

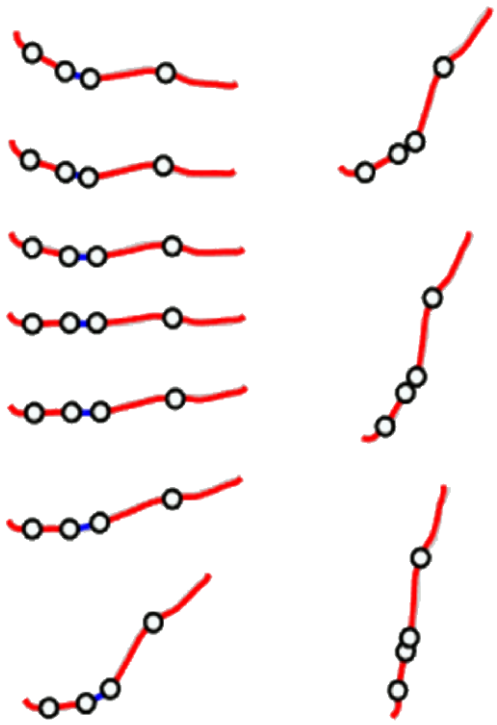

Figure 7. *The chain defined by* **V** *= [*$\mathcal{M}$ $\mathcal{M}$ $\mathcal{C}$ $\mathcal{M}$ $\mathcal{M}$*] and* **W** *= [*$\mathcal{R}$ $\mathcal{R}$ $\mathcal{R}$ $\mathcal{R}$*] matching the shape of the 10 target profiles. The red curves represent* $\mathcal{M}$*-segments, the blue curves represent* $\mathcal{C}$*-segments, and the white dots represent the revolute joints connecting adjacent segments.*

A final optimal SM was achieved after repeated calculation using different possible **V** and **W** vectors as inputs. The inputs used to generate this SM were **V** = [$\mathcal{M}$ $\mathcal{M}$ $\mathcal{C}$ $\mathcal{M}$ $\mathcal{M}$] and **W** = [$\mathcal{R}$ $\mathcal{R}$ $\mathcal{R}$ $\mathcal{R}$] (Figure 7). The resulting SM was:

$$SM = \begin{bmatrix} 121 & 164 & 113 & 334 & 321 \\ 121 & 164 & 102 & 334 & 321 \\ 121 & 164 & 123 & 334 & 321 \\ 121 & 164 & 118 & 334 & 321 \\ 121 & 164 & 126 & 334 & 321 \\ 121 & 164 & 134 & 334 & 321 \\ 121 & 164 & 122 & 334 & 321 \\ 121 & 164 & 89 & 334 & 321 \\ 121 & 164 & 82 & 334 & 321 \\ 121 & 164 & 60 & 334 & 321 \end{bmatrix}$$

with an associated EM:

$$EM = \begin{bmatrix} 0.4696 & 0.8610 & 0.8483 & 1.6620 & 2.1942 \\ 0.5749 & 0.5517 & 0.7036 & 0.7841 & 1.1676 \\ 0.6979 & 1.7560 & 2.0338 & 1.9482 & 1.7391 \\ 0.3662 & 0.7922 & 0.7922 & 1.3429 & 1.0508 \\ 0.4815 & 0.4345 & 0.4345 & 0.8161 & 1.8597 \\ 0.3040 & 0.4449 & 1.2080 & 1.4076 & 1.4076 \\ 0.2575 & 0.9715 & 0.4944 & 1.1542 & 1.1247 \\ 0.3736 & 0.8582 & 1.2201 & 1.2908 & 2.6364 \\ 1.1389 & 1.7650 & 0.5225 & 1.5277 & 1.9876 \\ 1.9159 & 1.0888 & 1.1604 & 2.1882 & 3.8294 \end{bmatrix}$$

which has a mean error value of 1.1728. The length of the 10 target profiles were defined by 1053, 1042, 1063, 1058, 1066, 1074, 1062, 1029, 1022, and 1000 pieces, respectively, with an average piece length of 0.1847.

Following generation of the SM, the linear pieces constituting each segment of the chain were then scaled about the origin of the pixel-based coordinate system in which they were defined to the size of the test subject's foot. This was accomplished by measuring the horizontal distance in inches between the two endpoint markers located respectively at the tip of the subject's hallux and the back of the subject's heel. This same distance was then measured in pixels from the design profile images. The ratio of the distance in inches and the distance in pixels yielded a scale multiplier (calculated to be 0.0479 inches per pixel) which was applied to the coordinate locations of the endpoints defining each piece, enlarging the segments to the proper size.

3.3 Solid Modeling of Links

Segment geometries were imported into Solidworks CAD modeling software and used to define 10 different curves (Figure 8), each corresponding to a configuration of the chain matching one of the target profiles. These curves were used to define the sectional profile of the bottom portion of each link. Note that for each of the curves in Fig. 8, only the positions and orientation of each segment, the angles between segments, and the arc length of the third segment (the *C*-segment) differ.

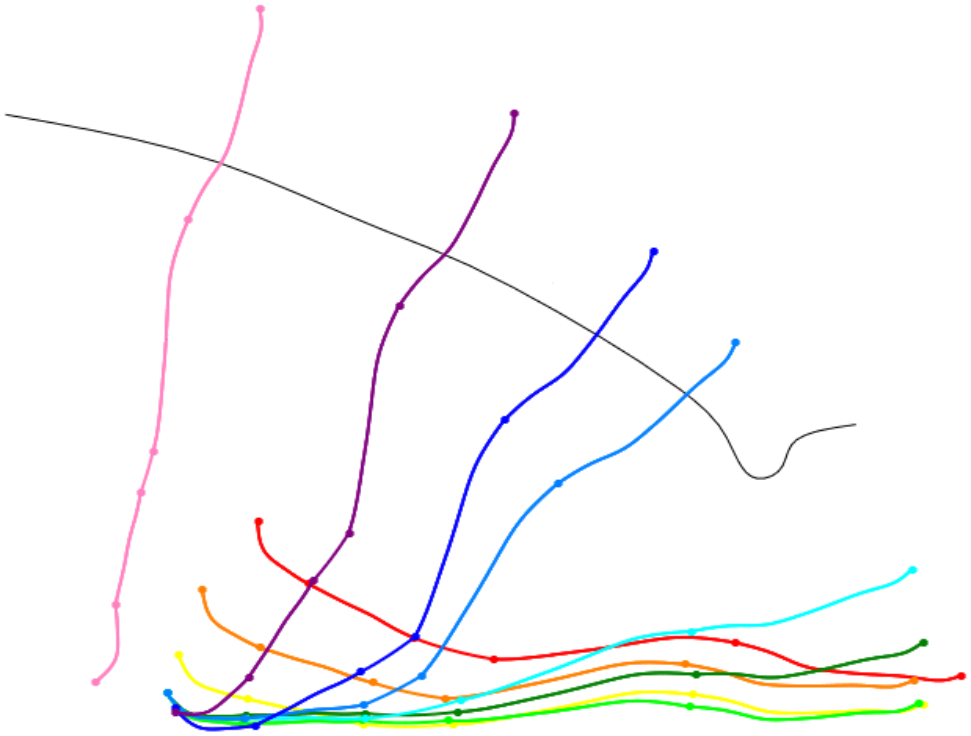

Figure 8. *10 configurations of the 5-segment geometry corresponding to each of the target profiles, beginning with the instant prior to initial heel strike (red) and ending with the instant just after toe-off (pink). The black curve represents the trajectory of the ankle measured from the design profile images.*

The fourth curve (light green in Fig. 8) was chosen as a reference configuration from which the rest of the geometry of each link would be constructed. While any of the configuration curves could have been chosen, the fourth curve corresponds to the midstance configuration, in which the bottom of the foot is in full contact with the ground, resulting in a nearly horizontal configuration in which the curve is approximately tangent to horizontal near both ends, providing a convenient reference axis.

Figure 9 shows the model of the foot in the nine configurations specified by the first 9 profiles. Note that the tenth configuration (defined by the pink curve in Fig. 8) was eliminated as a design objective for reasons discussed in Subsection 3.4.3. As a result, there is no configuration of the foot corresponding to this curve.

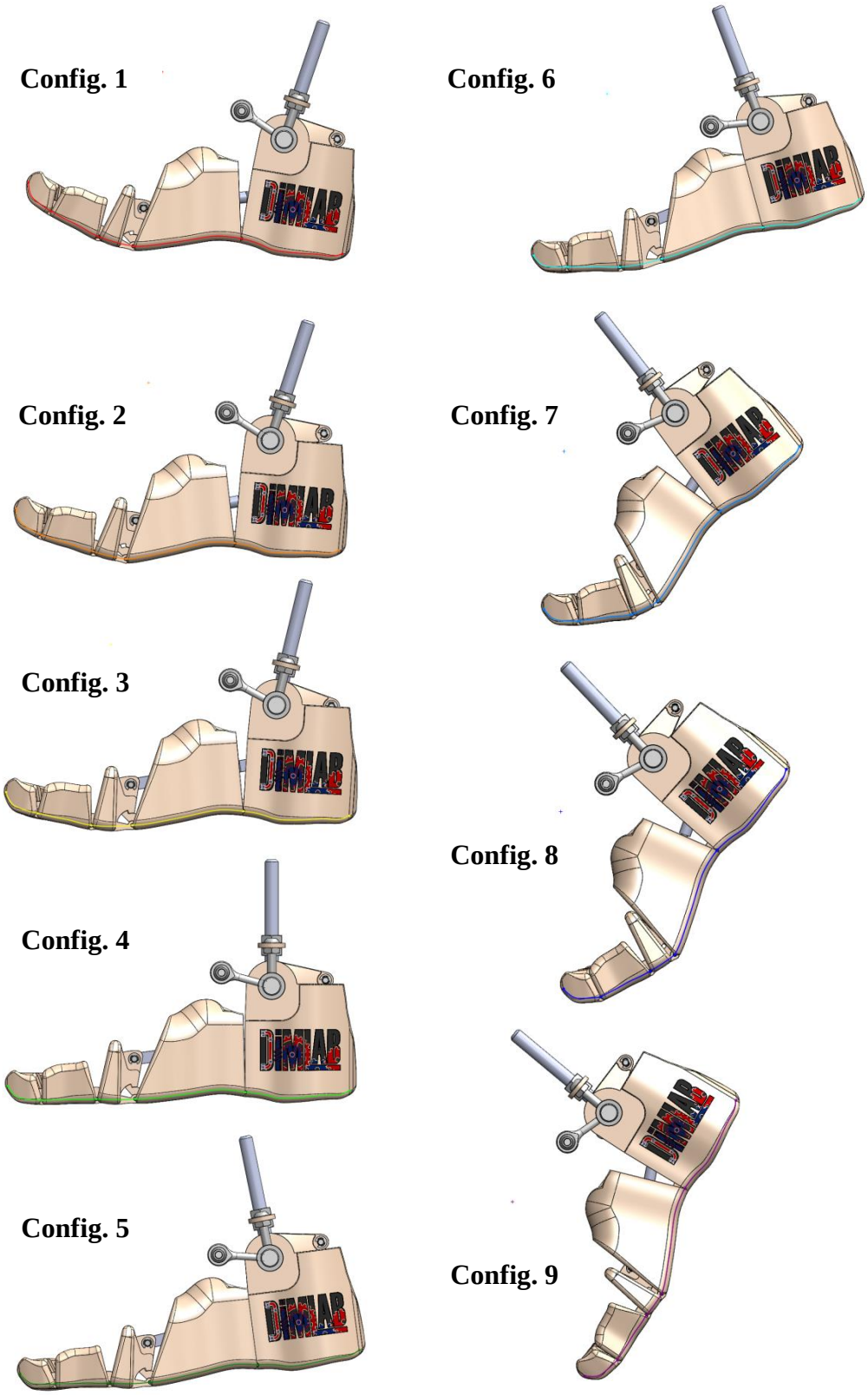

Figure 9. *Solid model of the foot in each of the nine configurations specified by the segment curves generated during segmentation.*

Figure 10 shows the five constructed regions of the foot, each corresponding to one of the segments in the rigid-body chain. Each region is comprised of one or more rigid links.

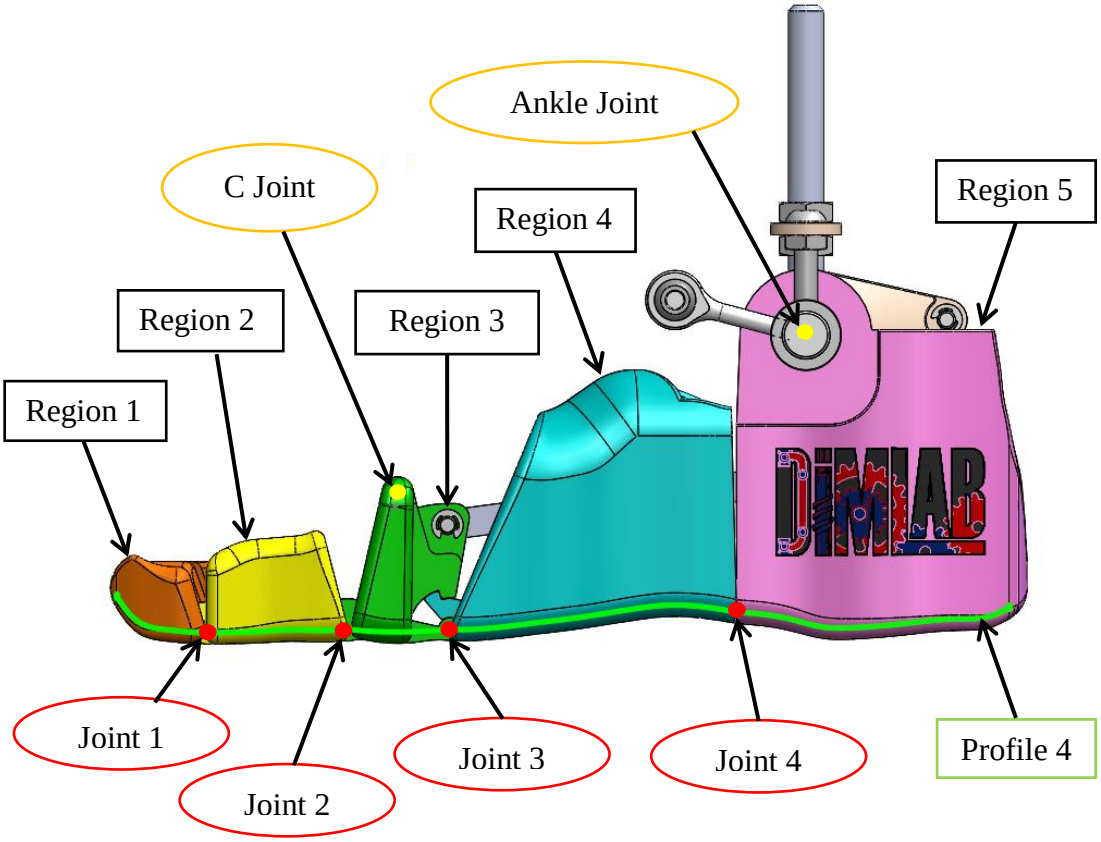

Figure 10. *Medial view of the solid model of the foot in the reference configuration showing the regions of the foot model corresponding to the calculated segment curves.*

Note that while the synthesized chain contains five segments, more than five links are required to achieve the shape of the profiles (a single *C*-segment, for example, generally consists of a two-link RPR chain). If the shank connection is considered a fixed frame, the foot consists of a total of 7 rigid links: one link in Region 1 (Links 1A and 1B shown in Figure 11 are counted as one, since they are designed to move interdependently); one link in Region 2; two links in Region 3 (Links 3A and 3B are also counted as one link); one link in Region 4; one link in Region 5; and one link constituting the fixed frame. The chain comprising the foot contains a total of 6 revolute joints and no higher order joints. Thus, by Equation 1, the design has 6 independent DOF.

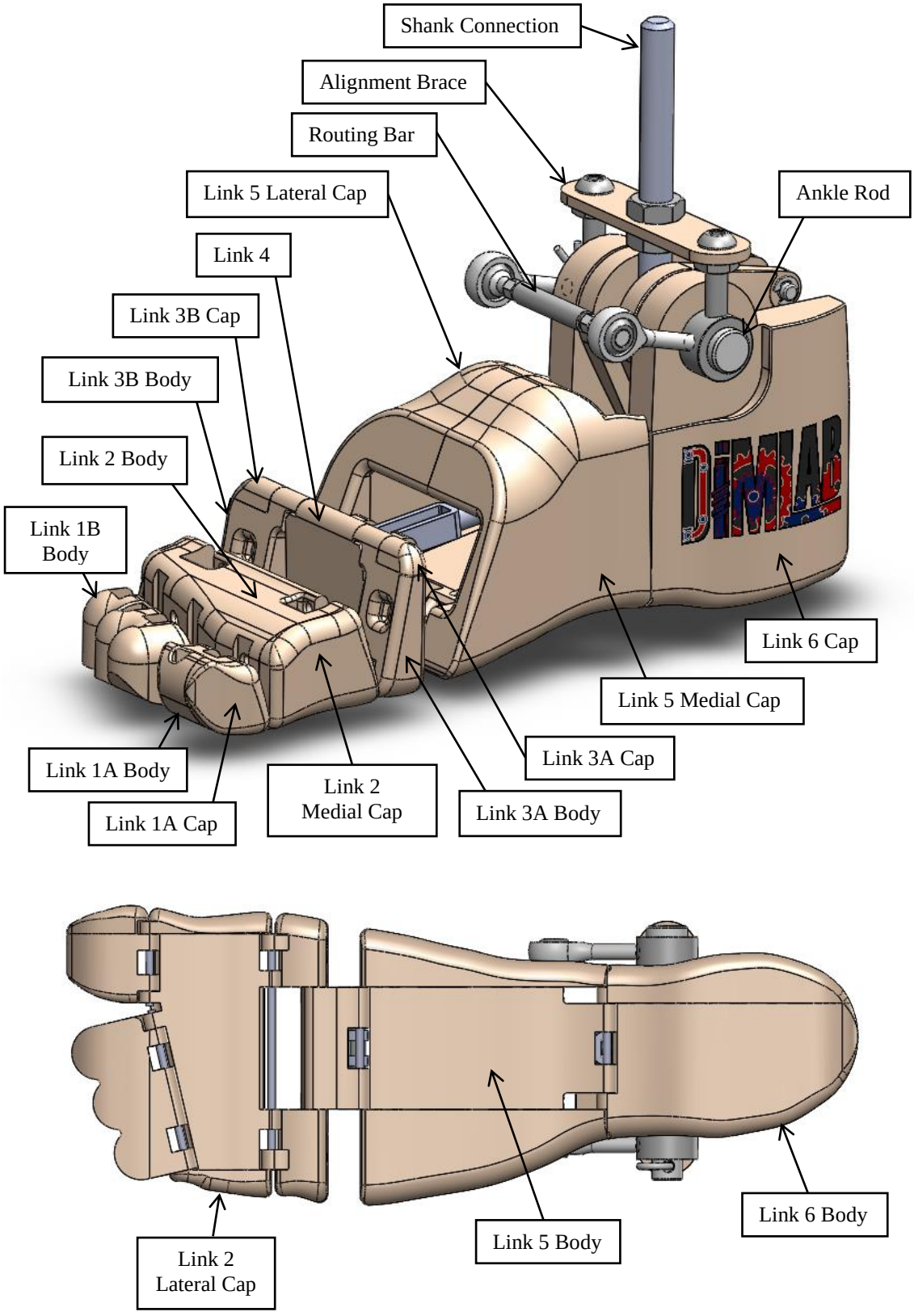

Figure 11. *Components of the foot.*

As can be seen in Fig. 11, each link of the foot except for Link 4 can be subdivided into two or more separate components. In general, each link consists of a main "body" component, and one or more "cap" components that retain the rod in each joint. Each cap component has two or more octagonal pegs on its inside face designed to be friction fit into corresponding holes on the body component. The fit is tight enough such that the body and cap components do not separate during use of the foot, yet loose enough to allow for removal of the cap components by hand if access to the joints is required. Henceforth, unless otherwise noted, "link" will refer to the combination of both a body component and its associated cap components.

3.4 Mechanical Design Considerations

The following subsections will each be dedicated to an aspect of the design of the links constituting the foot. Subsection 3.4.1 discusses the approximation of non-critical geometries. Subsection 3.4.2 details the design of the joints with consideration of actuation. Subsection 3.4.3 describes the strategy used to approximate the curvature specified by the *C*-segment. Note that the reader may find it helpful to consult Figure A2 in the Appendix for a visual depiction of the anatomical planes and axes of the foot referred to throughout these subsections.

3.4.1 Approximation of Non-plantar Geometries

The geometry of the plantar surface of the foot is of great importance in prosthetic foot design because of its influence on balance and weight distribution during stance. Less critical to these basic walking functionalities are the geometries of the dorsal, medial, and lateral surfaces, the reproductions of which in artificial feet are mainly for cosmetic purposes. Because functionality (i.e. adherence to the ROS) can be achieved without exactly conforming to these surfaces, the geometries defining these surfaces on the foot model were approximated.

A profile of the test subject's foot taken from the dorsal view was digitally identified from photographic data using the same MATLAB script employed in Section 3.1 to extract design profiles. This profile was similarly scaled and imported into Solidworks as a set of curves used to define non-critical link geometry. Small alterations to this profile,

however, were necessary in order to ensure practical partitioning of the foot into the five regions specified by the segment geometry obtained in Section 3.2.

Perhaps the most obvious of these alterations is the approximation of the geometries of the second through fifth toes. As can be seen in Figure 12, the second, third, and fourth toes all have the same width and have a uniform tip radius, while the fifth toe is absent entirely. The approximation of the toes is due in part to unclarity of the images from which the dorsal profile was extracted, as the presence of shadows between each toe made their exact shapes difficult to discern. Measurements taken of the subject's toes, however, revealed insignificant differences in the widths of the middle three toes. The length of each toe (exempting the hallux) was not measured, nor was the exact curvature of the tips of the toes. It was observed from the dorsal profile curves, however, that the tip of each of the three middle toes was arc-shaped, and that the relative decrease in length of the toes could be approximated by constraining the tip arcs to a straight line 157˚ counterclockwise from the frontal axis in the transverse plane. The geometries of the three middle toes were combined to form Link 1B instead of creating a separate link for each toe, which would have further increased the complexity of the foot mechanism. As a result, differences in the amount of pressure born by each of the middle toes due to their bifurcation were neglected.

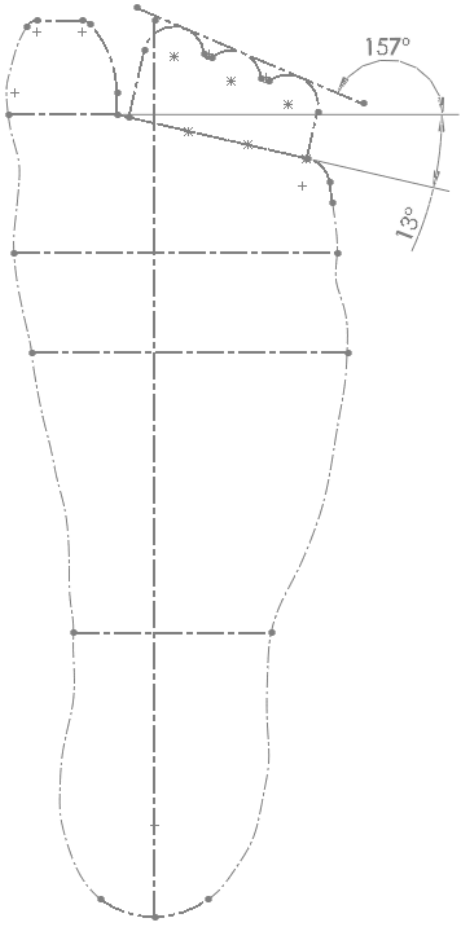

Figure 12. *Construction geometry and angles used to approximate toe shape in a dorsal profile of the foot.*

The omission of the fifth toe was dictated by a lack of available space. Because the locations of the joints along the target profiles were generated from data taken with respect to only one view of the foot, determination of the corresponding locations of these joints along a lateral profile of the foot could not be achieved without unwarranted speculation. In order to simplify joint structure, each joint was centered along an axis running straight across the foot parallel to the frontal axis. As a result of this simplification, however, it was observed that Joint 1 connecting Links 1A and 1B to Link 2 would run diagonally across the middle three toes (as can be visualized from Fig. 12), and would end at a location past the tip of the fifth toe. Due to the awkward design of the resulting frontal link, Region 1 was split into two separate links: Link 1A approximating the shape of the hallux, with a joint running across its width frontally, and Link 1B approximating the geometry of the three middle toes, with a joint running at an angle of 13˚ clockwise from frontal in order to better approximate the actual locations of the metatarsophalangeal joints about which these toes rotate when bent. A joint located along this secondary axis, however, would inevitably split the fifth toe, requiring yet a third link to capture the geometry of the tip of this toe. Because this toe bears comparatively little weight during stance, it was simply omitted, with a small portion of its outer geometry provided by the Link 2 lateral cap, which retains Link 1B.

The contours of the dorsal surface of the foot from the medial perspective were also approximated using non-plantar curves extracted from the design profile images. More creative liberty was taken with these contours than with those from the dorsal profiles, as a greater emphasis was placed on providing enough space to house internal components than on biological accuracy.

3.4.2 Joint Construction

A unique feature of a rigid-body foot design based on kinematic analysis is the method by which joints are located. Other segmented rigid-body foot prostheses containing revolute joints have traditionally placed joints at locations corresponding to biological joints in the foot. Rifkin, for example, developed a multi-segment foot device with joints located at positions corresponding to the metatarsophalangeal and talocalcaneal joints to achieve improved ambulatory function [45]. The positioning of joints in this work,

however, is completely independent of foot anatomy, and is instead determined during the segmentation process based on a single curved profile removed from the musculoskeletal geometry of the foot.

In order to determine the ranges of motion of the four synthesized joints, the relative angles between each segment in the optimized chain were measured in each configuration and used to determine a maximum angular deflection at each joint. Table 1 provides a summary of these measurements for the first nine configurations.

Joint	1	2	3	4
Config 1	15.96	12.53	19.10	11.76
Config 2	11.63	17.89	15.60	11.60
Config 3	19.00	14.15	33.24	8.79
Config 4	16.18	27.23	36.20	1.51
Config 5	**22.97**	**27.45**	32.63	0.00
Config 6	21.65	17.67	**36.44**	0.03
Config 7	14.83	0.00	6.27	15.31
Config 8	0.00	14.51	0.00	**17.62**
Config 9	8.75	22.56	9.43	16.96

Table 1. *Relative angular deflection (in degrees) at each joint in the first nines configurations. Values in bold denote the maximum angular deflection achieved at each joint.*

Each of the four joints was modeled as a crescent joint with a positional stop to prevent the joint from deflecting beyond the rotational limits specified in Table 1. The structure of a crescent joint is shown in Figure 13. It is important to note that the center of each joint about which the connected links rotate does not lie directly along the plantar curve defined by the configuration curves as was assumed during segmentation. Rather, the center of each joint is vertically offset 0.12 in. above its calculated position along the configuration curves. This is because it is problematic to create the structure for a crescent joint directly on the surface of the foot in contact with the ground, as the bottom portion of the central hub would extend past this surface.

The purpose of splitting each link into separate body and cap components is to retain the alignment rod concentrically aligning the central hubs of the anterior and posterior links associated with each joint. Each joint was constructed such that, to assemble the

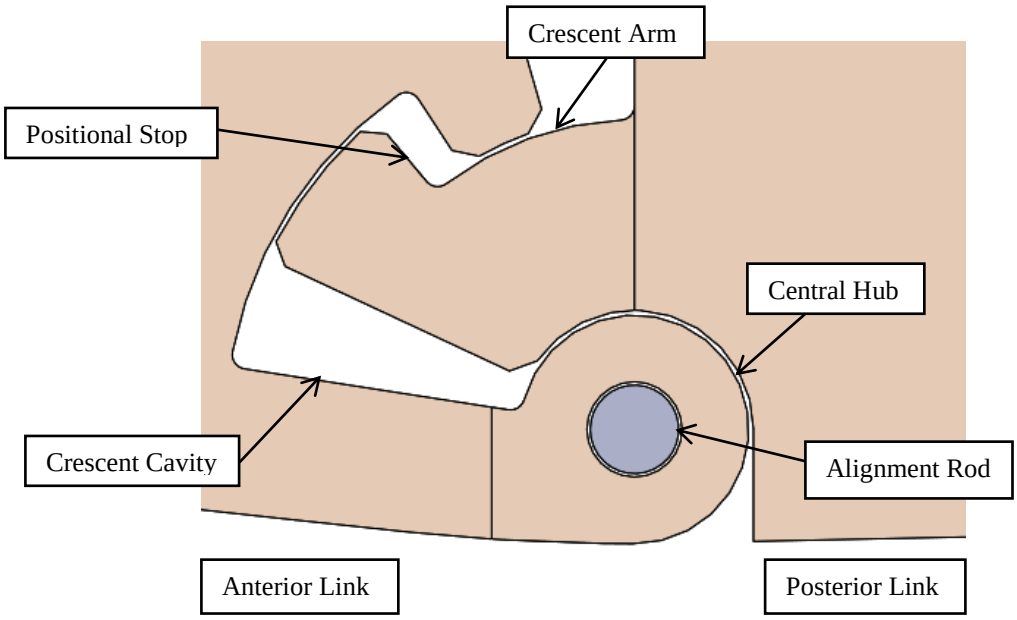

Figure 13. *Structure of a crescent joint.*

prototype, the crescent arm of the posterior body could be aligned with the cavity on the anterior body (such as shown in Fig. 13), allowing the posterior body to "slide into" the open cavity until hitting a stop at the far end of the joint. The stop on the opposite end of the foot is another central hub located either on the posterior body component (as is the case with the Joint 1 connecting Links 1A and 1B to Link 2) or on the lateral side cap component of the posterior link (as is the case with Joints 2, 3, and 4). The joints are aligned by inserting the alignment rod through the central hubs on both anterior and posterior bodies. The rod is retained within the joint by finally attaching the medial side cap components to their respective body components.

In anticipating of actuation elements, each joint contains one or more spaces cut through the central hub, crescent cavity, and crescent arm to accommodate one or more torsional springs. These spaces are most clearly visible from the plantar view of the foot in Fig. 11. Small torsion springs can be compressed and inserted into these spaces before insertion of the alignment rod, which passes through the centers of the torsion springs as it passes through the central hub. The incorporation of torsion springs is discussed in more depth in Section 3.5.

3.4.3 Approximation of *C*-segment Curvature

As mentioned previously, curved prismatic joints are often avoided when possible in practical design due to the requirement of tight manufacturing tolerances and surface finishes. In addition, there is a relatively high chance of the joint binding due to accumulation of debris within the joint, as a portion of the sliding surface is exposed when the joint extends, and experience reveals that passively driven prismatic joints are often difficult to control. Perhaps the greatest detriment of the use of passive prismatic joints for prosthetic applications, however, are the large size requirements of a sliding linkage, particularly if there is a significant difference in arc length between the fully extended and fully contracted configurations.

Measurement of the target profiles revealed that the *C*-segment had a minimum arc length of 60 pieces (0.5513 in.) in the tenth configuration (corresponding to the instant just after toe-off) and a maximum arc length of 134 pieces (1.2313 in.) in the sixth configuration (corresponding to the portion of terminal stance during which weight is transferred from the ball of the foot toward the toes). Thus, an RPR chain embodying the *C*-segment would have to contract to a length less than half the length of one of its links while confined to a relatively short region of the foot. For this reason, as well as the fact that plantar geometry directly after toe-off is irrelevant for characterizing walking during the stance phase, the tenth configuration was eliminated as a design objective.

A different embodiment of a *C*-segment than an RPR chain was employed to further save space. This embodiment was a chain comprised of two links with an equal radius of curvature joined by a revolute joint at the common center of curvature. However, this embodiment also proved to be problematic, as the *C*-segment had an average radius of curvature of 4.9585 in. (corresponding to the red curve in Figure 14), meaning that the center of curvature needed to locate the revolute joint lay approximately 3 in. above the dorsal surface of the foot. To reduce this distance in order to achieve a centerpoint located within the contours defining the dorsal surface, the radius of curvature of the two links constituting the *C*-segment was reduced to 1.62 in. (corresponding to the blue curve in Fig. 14) In order to approximate the shallower arc specified during segmentation, the

C-segment links were constructed such that the bottom surfaces of these links remained tangent to the unoffset segment curve in each configuration (Figure 14).

The final embodiment of the *C*-segment (Region 3) consists of two links: an inner link (Link 4) and an outer pair of links (Links 3A and 3B) located to either side of Link 4 (refer to Fig. 11 for clarity). Link 4 is connected to Link 5 at Joint 3, and Links 3A and 3B are connected to Link 2 at Joint 2. Links 3A, 3B, and 4 are joined at the common centerpoint of curvature located at the C Joint (the blue dot in Fig. 14). The C joint is similar in construction to Joints 2-4 in that it contains an alignment rod which keeps Link 4 aligned concentrically at the point of rotation with Links 3A and 3B. Links 3A and 3B each contain a small cap piece at their shoulders which retains the rod. Like each of the crescent joints along the bottom of the foot, the C Joint contains positional stops which keep Links 3A and 3B and Link 4 from extending past the angle of deflection which produces the maximum arc length achieved at full extension in the fifth configuration.

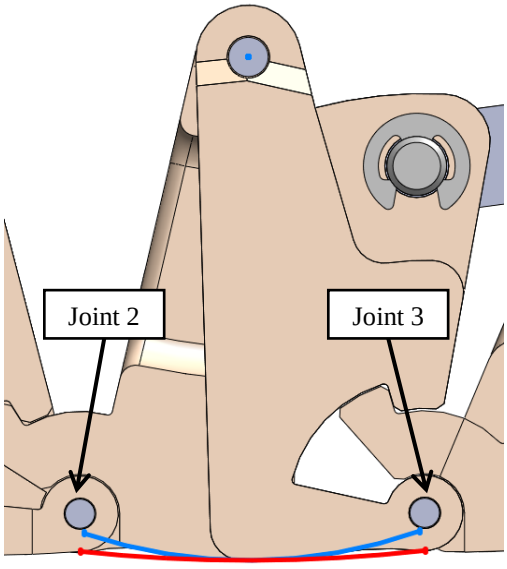

Figure 14. *Approximation of C-segment curvature (red) using a reduced radius of curvature (blue) to define link geometry.*

Links 3A, 3B, and 4 were designed such that the bottom surface of at least one of the links is in contact with the ground in configurations 2-6. Thus in the former configurations when the forefoot is unflexed, weight at the ball of the foot would be born by Link 4, and in the latter configurations when the forefoot is dorsiflexed, weight at the ball of the foot would be distributed amongst Links 3A and 3B.

3.5 Development of a Tendon-based Actuation Scheme

Perhaps the greatest challenge offered by this design is how to actuate and synchronize 6 independent DOF. Examination of the configuration-to-configuration angles for the joints contained in Table 1 reveals that each joint moves in an independent sequence of

clockwise and counterclockwise rotations, often changing direction rapidly between configurations. While it is possible that with adequately stiff joints the foot may be functional without active elements, the resulting rotation in each of the joints defining the change in shape of the foot would almost certainly fail to produce the configurations specified by the design profiles, rendering the exercise of synthesizing the rigid-body chain irrelevant. Thus, in order to ensure the foot achieves each configuration, each joint must be actuated independently.

Tendon-based actuation schemes for prosthetic and robotic limbs have risen in popularity in recent years, particularly in the design of artifical hands [46-48]. Despite the physiological similarities between the function of the tendons in the hand and those in the foot, tendon-driven foot devices appear scarce by comparison. Still, there is some precedent for tendon-driven feet. The joints in Rifkin's foot [45] are driven by tensegrity structures comprised of small wire ropes in tension, which facilitate tendon-like motion. Ficanha, Rastgaar, and Kaufman also developed a cable-driven foot mechanism capable of achieving plantarflexion and dorsiflexion, as well as inversion and eversion using tendon-like cables [49].

As mentioned in Subsection 3.4.2, Joints 1-4 were designed to accommodate the insertion of torsion springs in order to provide the foot with appropriate stiffness to provide basic energy storage and return. Inclusion of an energy storage and return mechanism was desired in consideration toward future adaptation of this design for prosthetic use. The inclusion of springs at each joint keeps the foot in a neutral position of plantarflexion, as shown in Figure 15. A series of tendon-like cables in tension could then be attached to each of the links to overcome the spring force, and by adjusting the amount of tension in each cable, the necessary degree of dorsiflexion required to match each configuration could be achieved. Choosing the plantarflexed configuration as the neutral configuration simplifies the actuation

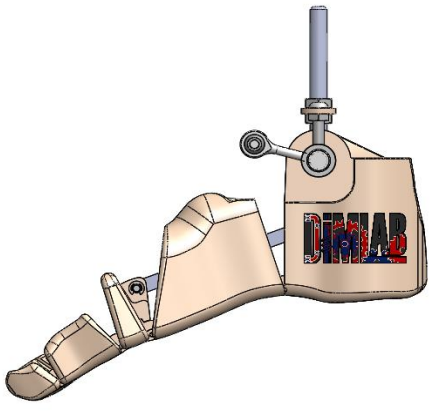

Figure 15. *Solid model of the foot in the plantarflexed configuration.*

scheme by eliminating the need for an antagonistic set of tendons to achieve plantarflexion, reducing the overall number of tendons required for actuation.

Figure 16 shows the routing scheme of the cables. Each cable is connected to a link and is routed through a series of channels built into the subsequent links that guide the cables upward and around the routing bar. The routing bar is fixed to the shank connection such that each cable moves relative to the same fixed frame. Cables of the same color correspond to a common DOF and are meant to be coupled such that the motion of each pair of cables can be achieved with a single actuator. Note that with the exception of the single cable at the heel (magenta in Fig. 16), there is at least one pair of cables dedicated to each region of the foot. A pair of cables is used for each region in order to more evenly distribute the tension force imparted by each set of cables on their corresponding links, as well as to reduce the total amount of tension required of each individual cable. Note that due to its position, the cable pair controlling Link 6 passes under and around the routing bar from the opposite direction as the other cables. Also note that the two red cables in Fig. 16 each connect to separate links (1A and 1B). Since it is desired the motions of Links 1A and 1B be independent, these cables are to be controlled in such a way as to synchronize the motion of the two links, effectively accounting for one DOF. Similarly, the yellow pair of cables controls the interdependent motion of Links 3A and 3B, with one cable connecting to

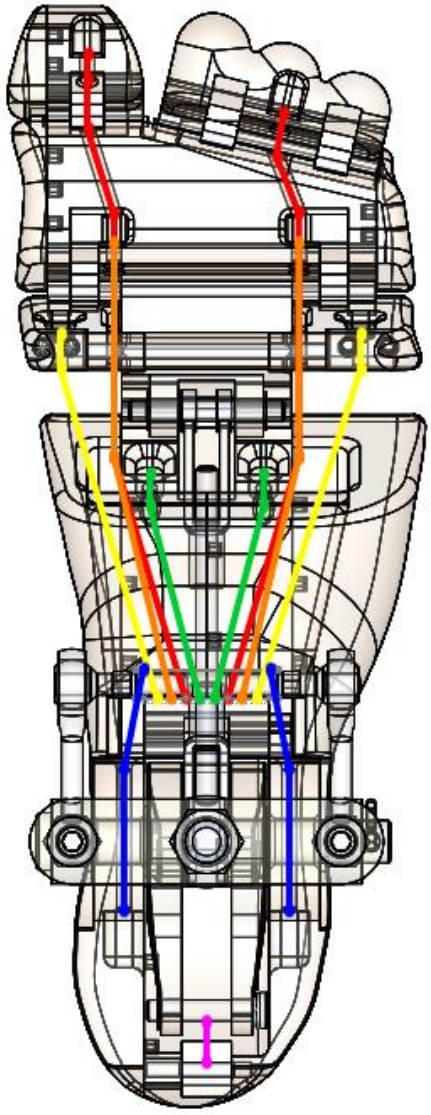

Figure 16. *Routing scheme for the tendon-like cables acting in tension on each link of the foot.*

each of the two links, accounting for the rotational DOF at the C joint. The rotation of Link 4 about Joint 3 is controlled via the single magenta cable at the heel, which attaches to a bell crank mechanism that connects Link 4 via a coupler (Figure 17).

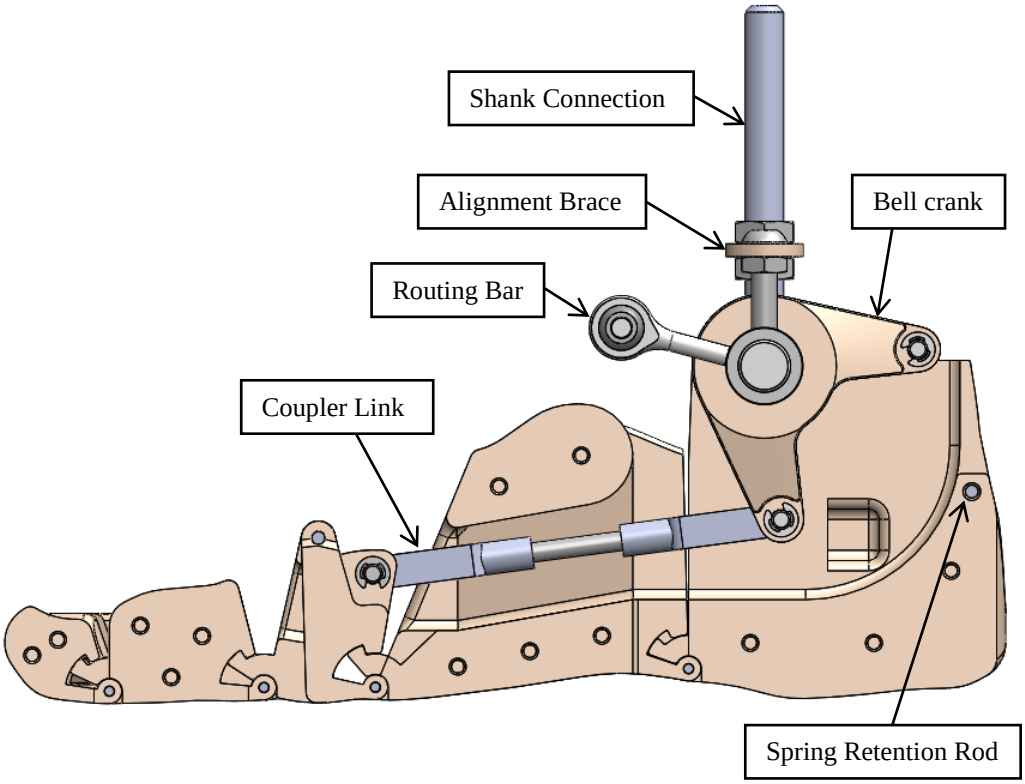

Figure 17. *Cross-sectional view of the foot interior showing the bell crank mechanism used in the actuation of Link 4.*

The design of the bell crank mechanism is inspired by two different ankle-foot devices. The first is an artificial foot developed by Collins and Kuo [50] designed to restore a portion of the energy lost due to collision via a clutch mechanism which releases energy stored in a compression spring during ankle push-off, reducing ankle work. The second device is an orthosis developed by Collins, Wiggin, and Sawicki [51] based on a similar principle. A ratchet and pawl clutch mechanism attached to a band worn on the calf provides tension to an extension spring at the back of the heel while the foot is in contact with the ground, and then disengages during push-off, releasing the stored energy in the spring. Both of these designs are displayed in Figures 18a and 18b, respectively.

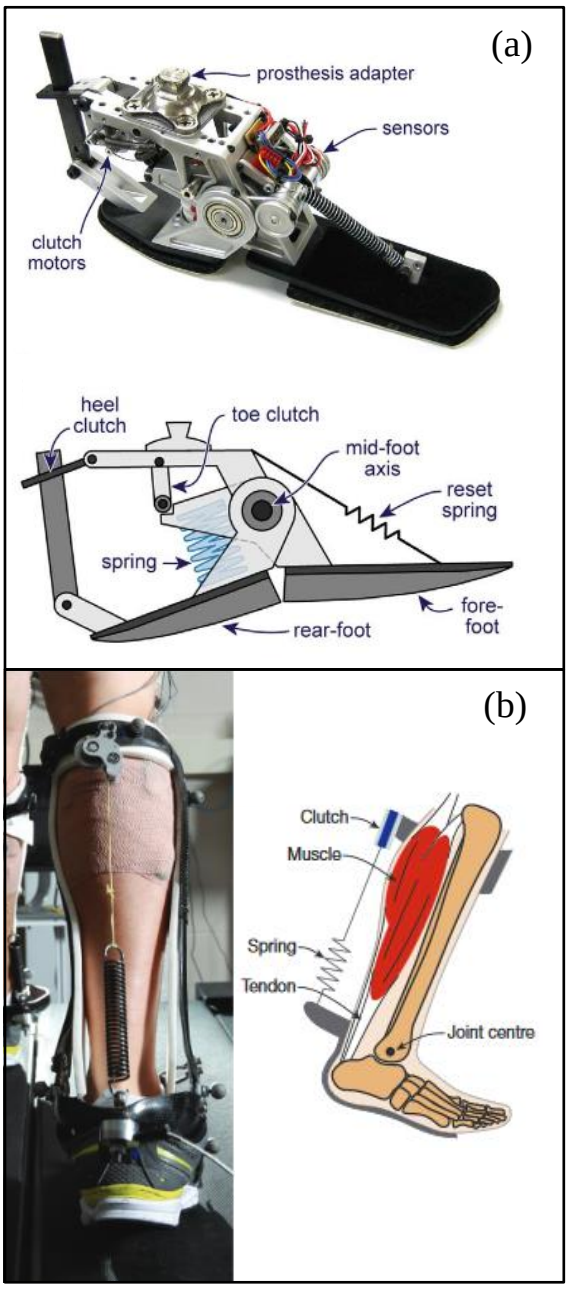

Figure 18. *Images and diagrams of an energy restoring (a) artificial foot and (b) orthosis used as inspiration for the design of the bell crank mechanism. Images adapted from Refs. [46] and [47], respectively.*

Table 1 reveals a large change of angle in Joint 3 between the sixth and seventh configurations as weight is shifted to the forefoot. The resulting motion would force Links 3A and 3B and Link 4 to contract, pushing the coupler link back toward the heel, rotating the bell crank at the ankle counterclockwise. An extension spring connected to the opposite side of the bell crank anchored to the heel by the spring retention rod would then be forced to extend, absorbing energy otherwise lost during the contraction of the forefoot. The magenta cable attached to the same end of the lever as the spring could be timed to release tension abruptly during the push-off period between configurations 8 and 9, releasing the energy stored in the spring, rapidly forcing the coupler forward and causing Link 4 to snap back clockwise to account for the change in angle between the eighth and ninth configurations. Thus, the bell crank mechanism would store energy in the same fashion as the orthosis in Fig. 18b, and release it during push-off in a manner similar to Collins and Kuo's artificial foot in Fig. 18a.

Full realization of the conceptualized actuation scheme for this foot ultimately lay beyond the focus of the project objective. After redirection at the routing bar, it was envisioned that the cables would run up the shank to a winch-like mechanism driving a series of cams that would wind and unwind the cables to increase and release tension in each cable

pair as dictated by the required degree of dorsiflexion opposing the spring-driven plantarflexion specified by the joint angles. The rotation of each cam would be driven by one or more small motors, the speed of which could be determined through the use of a robust controller capable of adapting the speed of the motor based on the speed of the user's walk. The design of such a controller, however, is currently outside the scope of this project. At present, the tension in each cable must be adjusted manually.

It should be noted that the bell crank mechanism was also not fully implemented. An extension spring was installed at the heel that allows the motion of Link 4 to be actuated by pushing upward on the arm of the bell crank as envisioned. A mechanism similar to the clutch used in the above orthosis to facilitate the rapid release of the cable at the heel, however, has not yet been created. As a result, the prototype in its current state does not have an energy storage and return mechanism to assist in push-off other than the innate stiffness provided by the torsion springs in Joints 1-4.

3.6 Development of Prototype and Recommended Modifications

A physical model of the design detailed in the above sections was rapid prototyped (Figure 19). The cap and body components constituting each link were 3D printed using ABS thermoplastic. ABS is a common material used in 3D printing, which offers acceptable rigidity, is easily thermoformed, and possesses a good strength-to-weight ratio. While ABS has successfully been used to create 3D printed prostheses, there is a concern regarding the suitability of ABS to this design in terms of strength given the material thinness in certain weight bearing structures, particularly in the crescent joints. Given that this project emphasized shape-change over prosthetic functionality, material selection was guided more by cost and availability than by consideration of potential biomechanical loading. As a result, the author recommends a stronger material be considered in future iterations of this design, such a polypropolene-based copolymer, as was recommended by Sam et al. in the design of the S&R foot [20].

In addition to the foot itself, a benchtop support stand that allows the foot to achieve each of the nine target configurations was fabricated. The support stand features an adjustable height cross member to which the foot can be mounted via the threaded shank

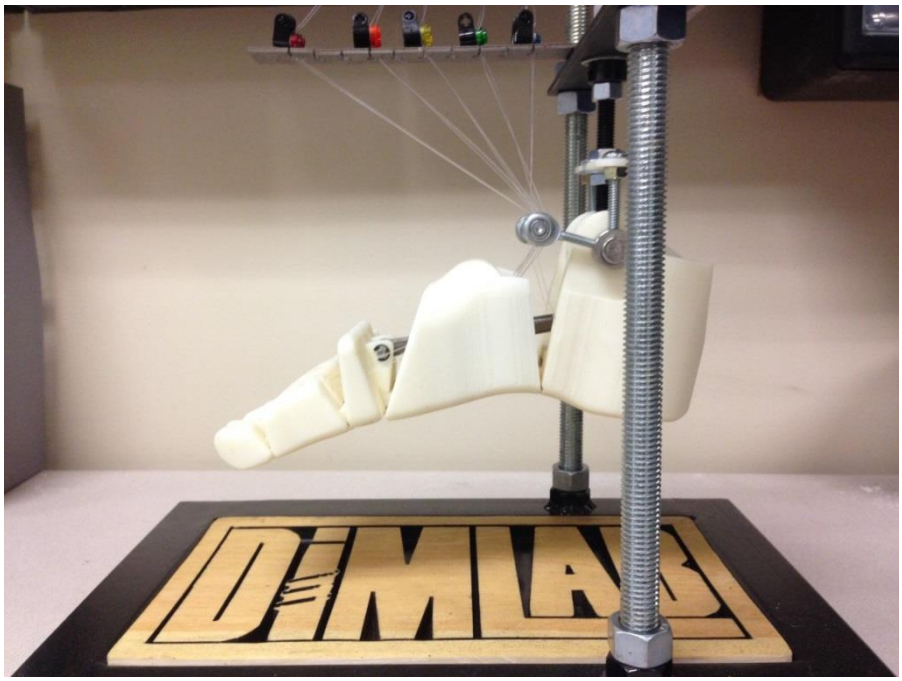

Figure 19. *Prototype of the foot and support stand.*

connection. Thus the foot is suspended with the shank fixed and is rotated about the ankle to achieve each configuration. A thin cantilevered plate anchored perpendicular to the center of the cross member sits above the foot. The plate has slots cut out from the side leading to a row of ten small holes drilled in the center of the plate at 0.25 in. intervals. Each of the five pairs of cables controlling one region of the foot can be slid through one of the ten slots into the corresponding hole. A terminal at the end of the cable keeps the cable from sliding down through the hole, keeping the foot suspended. The tension in each pair of cables can be adjusted by attaching the terminals at different lengths along the cable, making it shorter or longer. Once all cables are adjusted such that the foot is suspended in the neutral configuration, the tension in the cables can be refined to provide the appropriate degree of dorsiflexion in each joint specified by the desired configuration by manually pulling the correponding cables, relocating a cable to a more distant hole, or a combination of both.

The cables initially used in the prototype were nylon monofilament wire rated at a test load of 30 lbs, well under the maximum tension induced by the light weight of the links and enough to overcome the spring force imposed by the torsion springs. While these cables were suitable for the purpose of actuating the suspended foot into the target

configurations, it was noted that the cables had a tendency to stretch after repeated use, thus requiring periodic relocation of the terminals along the cables. In addition, some relative motion between links was observed. For example, when pulling the pair of cables connected to Link 2, which route through Links 3A, 3B, 4, and 5, these links also displayed a tendency to move along with Link 2. In order to combat this unwanted motion, Joints 1-4 were each equipped with an increasing number of torsion springs acting in parallel such that Joint 1 had the lowest stiffness, while Joint 4 had the highest. The springs were arranged in this fashion such that by applying tension to the pair of cables connected to a specific link or set of links, the intended links would begin to rotate before reaching the tension required to overcome the larger spring forces in the subsequent regions, resulting only in motion of the intended links. Despite this progressive stiffening of joints, some relative motion hindering the foot's ability to smoothly achieve each configuration was still observed. For this reason, it is recommended that the current nylon cables be replaced with stranded, sheathed pull cables. The presence of a sheath around the cable would eliminate friction between the routing channel surfaces and the moving cable, thus helping prevent undesired motion of neighboring regions.

A final observation on the prototype is that the plantarflexed configuration chosen as the neutral configuration does not provide the proper degree of resistance required to oppose cable tension as was originally assumed. In order to mimic true plantarflexion, Links 3A and 3B and Link 4 would need to contract to their smallest effective arc length. However, in order to oppose cable tension in the neutral configuration, these links would need to be extended to their maximum effective arc length such that when additional tension is applied to the cables, these links contract. In the current plantarflexed position, these links are already fully contracted. Due to greater limitations in space at the C joint, torsion springs could not be implemented at this joint in the same fashion as Joints 1-4., leaving the cable force currently unopposed. The design can more easily be adapted to accommodate a pair of compression springs mounted to the anterior surfaces of Link 5 that push against the opposite surfaces on Links 3A and 3B, keeping these links maximally extended in the neutral configuration. It is recommended that such springs be incorporated in future iterations of the design.

4 DISCUSSION

This chapter provides a discussion-based analysis of the final prototype and its potential for use as a prosthesis. Section 4.1 addresses the functional limitations of the current design and presents an overview of the requirements needed to repurpose the design for prosthetic use. Section 4.2 presents some novel ankle-foot design implications stemming from this work. Recommendations for future work toward addressing the requirements enumerated in Section 4.1 are presented in Section 4.3.

4.1 Limitations

As previously stated, the primary purpose of this work was the embodiment of a mechanical foot design capable of replicating the change in shape of the foot during walking. The limitations of the prototype in regard to accomplishing this goal have already been discussed in Section 3.6. However, there are further limitations to the functionality of the device as a practical foot mechanism. The device was not originally conceived as a prosthesis, but given the natural application of such an artificial foot, as well as the heavy usage of prosthetic design principles as inspiration for the design, there is a potential that the current prototype could be modified to fulfill the purpose of a prosthesis. In order to achieve minimum functionality as a prosthesis, a number of factors must first be addressed.

First and perhaps foremost is the fulfillment of the actuation scheme presented in Section 3.5. In order to properly attune such a complex actuation mechanism, further research on the biomechanical behavior of the foot is required, particularly in regards to characterizing the stiffness of the foot. The torsion springs currently implemented in the design are incapable of accurately representing the stiffness of the physiological foot and were chosen primarily for their small size. The use of photographic data alone is not enough to infer a proper stiffness. Traditionally, stiffness is characterized experimentally utilizing center of pressure and GRF data. No such data exists, however, for the foot used to generate the design profiles in this work. A further complication is that stiffness elements in the current design are limited to implementation at the joints, which do not necessarily correspond to locations of physiological joints in the foot for which biological

data already exists. While methods of characterizing the stiffness of a prosthetic foot at off-joint locations utilizing mathematical models or previously generated data exist [52, 53], these methods are generally better suited for design of single-body compliant feet. Olesnavage and Winter developed a method [54] for optimizing stiffness of the metatarsal and ankle joints of a rigid-body foot using pre-published gait data [55]. The methods outlined in Olesnavage and Winter's work could potentially be extended to this project if the GRFs and locations of center of pressure could be synchronized with the times at which design profiles were extracted. From there, basic static force analysis could be employed to determine an approximate local stiffness for each joint. Further investigation into the work presented in Ref. [54] is required to assess its applicability as a basis for spring selection.

A second requirement is quantitative test data characterizing the gait produced by the prototype, as well as its ability to withstand realistic biomechanical loading. It was postulated in Chapter 1 that a closer replication of the actual geometry of the foot would produce an ROS approximately symmetric to that of the physiological foot. While the literature seems to support this idea, center of pressure data from the prototype is needed to assess the validity of this claim. In addition to functional achievement of the ROS, the foot must also be able to safely support the weight of a user. Towards this end, selection of a stronger material may be required for the reasons enumerated in Section 3.6.

Consideration must also be given toward the experience of the prosthetic user. A biomechanically accurate prosthesis is ultimately unavailing if said prosthesis is not comfortable and convenient for the user. Aesthetically, the prototype may be improved by the inclusion of a cosmesis, which in addition to enhancing the appearance of the design, may also provide the advantages associated with elastic, skin-like compliant materials typically used in the molding of cosmeses such as silicone or polyurethane rubbers, which include increased abrasion resistance and shock absorption [56].

4.2 Implications for Design of Ankle-foot Devices

While the prototype in its current state may not be suitable as a prosthesis, the use of shape-changing kinematic synthesis to achieve biologically generated inputs presents

some novel implications for the design of ankle-foot devices. The use of methods of kinematic synthesis circumvent the need for prior characterization of the exact loading the device will be subjected to, instead relying on foreknowledge of the required positional configurations, which are often known in advance and are simpler to characterize, theoretically accelerating the design process and widening the design space.

While the design space in this project was limited to ten design profiles (later reduced to nine), the methods employed to generate a suitable rigid-body chain are applicable to any number of profiles of any curvature or arc length. This implies a potential to match additional shapes resulting from other foot functions beyond gait, such as running or kicking, all with a single rigid-body chain. Provided the challenges of actuating the resulting chain are met, employment of this design strategy could produce drastically more versatile and multifunctional ankle-foot devices. The ability to match multiple unique design profiles also suggests that a rigid-body chain possesses the ability to match design profiles generated by multiple individuals. As it applies to prosthetics, this signifies the potential existence of a single, mass reproducible prosthesis able to accommodate multiple users with similar effective foot geometries. Such a prosthesis could help alleviate the high costs associated with custom fabrication of more sophisticated designs.

4.3 Future Work

It is strongly recommended that future work focus on addressing the limitations identified in Section 4.1, and following through with the identified suggestions for further investigation. While the issues associated with the current prototype outlined in Section 3.6 should be addressed, immediate redesign of the foot beyond these relatively simple modifications is not recommended at this time, as it is anticipated that findings stemming from investigation into the literature recommended above may result in further alterations to the design.

Realization of a viable actuation scheme is of top priority, be it the one proposed in Section 3.5 and partially implemented in the current prototype or an alternative mechanism. Toward this end, preliminary steps in applying the Winter data [55] to a

static analysis of the foot in order to characterize the required stiffness of joints have already been taken. Following identification and implementation of suitable stiffness elements at each joint, evaluative testing will be conducted to assess the ability of the design to produce a physiologically accurate ROS.

5 CONCLUSION

This work outlined a design process based on methods of shape-changing kinematic synthesis resulting in the prototyping of a multi-segment rigid-body foot mechanism capable of matching the change in shape of the foot during walking. Design profiles representing the configurations of the foot to be matched by the mechanism were extracted from digital imagery of a test subject in gait. These profiles were approximated as a series of piecewise linear curves used to define the geometries of segments of a single, optimized mechanical chain able to approximate the shapes of the design profiles. The generated geometry of the chain was then used to define curvatures of the plantar surfaces of each rigid-link embodying the chain in a solid model of the design. A tendon-driven actuation scheme capable of driving the model into each of the design configurations was conceptualized. The model was rapid prototyped and a benchtop frame used to suspend the prototype was fabricated. The tendon-driven actuation scheme was partially realized using monofilament nylon cables in tension to oppose the force of torsional springs in the joints keeping the foot in a neutral, plantarflexed position.

The potential adaptation of the foot mechanism for prosthetic use was discussed, limitations of the prototype were identified, and suggestions for potential modifications to the current design towards addressing these limitations were presented. Implications for the design of ankle-foot devices using the methods of shape-changing kinematic synthesis employed in this work were also mentioned. Finally, recommendations for future work stemming from this project were made, including implementation of a full actuation scheme, a potential method of evaluating local stiffnesses for each joint, and biomechanical evaluation of the prototype based on the roll-over shape.

References

[1] Saltzman, C. L., and Nawoczenski, D. A., 1995, “Complexities of Foot Architecture as a Base of Support,” Journal of Orthopaedic & Sports Physical Therapy, **21**(6), pp. 354–360.

[2] Hedayati, R., Shargh, M. H., Soltani, T., Saeb, M., Ghorbani, R., and Hajihasani, A., 2014, “The Relation between Clinical Measurements of Plantar Characteristics and Static and Dynamic Balance Indices,” Middle East Journal of Rehabilitation and Health, **1**(2).

[3] Rodgers, M. M., 1995, “Dynamic Foot Biomechanics,” Journal of Orthopaedic & Sports Physical Therapy, **21**(6), pp. 306–316.

[4] Hansen, A. H., and Childress, D. S., 2010, “Investigations of Roll-over Shape: Implications for Design, Alignment, and Evaluation of Ankle-Foot Prostheses and Orthoses,” Disability and Rehabilitation, **32**(26), pp. 2201–2209.

[5] Morawski, J.M., and Wojcieszak, I., 1977, "Miniwalker -- A Resonant Model of Human Locomotion," *Biomechanics VI-A*, University Park Press, Baltimore, MD (1978): pp. 445-451.

[6] McGeer, T., 1990, “Passive Dynamic Walking,” The International Journal of Robotics Research, **9**(2), pp. 62–82.

[7] Perry, J., 1992, *Gait Analysis: Normal and Pathological Function*, Slack Inc., Thorofare, NJ.

[8] Collins, S. H., Wisse, M., and Ruina, A., 2001, “A Three-Dimensional Passive-Dynamic Walking Robot with Two Legs and Knees,” The International Journal of Robotics Research, **20**(7), pp. 607–615.

[9] Hansen, A. H., Childress, D. S., and Knox, E. H., 2004, “Roll-over Shapes of Human Locomotor Systems: Effects of Walking Speed,” Clinical Biomechanics, **19**(4), pp. 407–414.

[10] Hansen, A. H., and Childress, D. S., 2005, "Effects of Adding Weight to the Torso on Roll-over Characteristics of Walking," Journal of Rehabilitation Research & Development, **42**(3), pp. 381–390.

[11] Hansen, A. H., and Childress, D. S., 2004, "Effects of Shoe Heel Height on Biologic Roll-over Characteristics during Walking," Journal of Rehabilitation Research and Development, **41**(4), p. 547.

[12] Wang, C. C., and Hansen, A. H., 2010, "Response of Able-Bodied Persons to Changes in Shoe Rocker Radius during Walking: Changes in Ankle Kinematics to Maintain a Consistent Roll-over Shape," Journal of Biomechanics, **43**(12), pp. 2288–2293.

[13] Curtze, C., Otten, B., Hof, A. L., and Postema, K., 2011, "Determining Asymmetry of Roll-over Shapes in Prosthetic Walking," The Journal of Rehabilitation Research and Development, **48**(10), p. 1249.

[14] Ruina, A., Bertram, J. E. A., and Srinivasan, M., 2005, "A Collisional Model of the Energetic Cost of Support Work Qualitatively Explains Leg Sequencing in Walking and Galloping, Pseudo-Elastic Leg Behavior in Running and the Walk-to-Run Transition," Journal of Theoretical Biology, **237**(2), pp. 170–192.

[15] Adamczyk, P. G., Collins, S. H., and Kuo, A. D., 2006, "The Advantages of a Rolling Foot in Human Walking," Journal of Experimental Biology, **209**(20), pp. 3953–3963.

[16] Adamczyk, P. G., and Kuo, A. D., 2013, "Mechanical and Energetic Consequences of Rolling Foot Shape in Human Walking," Journal of Experimental Biology, **216**(14), pp. 2722–2731.

[17] Dumas, R., Chèze, L., and Verriest, J.-P., 2007, "Adjustments to McConville et Al. and Young et Al. Body Segment Inertial Parameters," Journal of Biomechanics, **40**(3), pp. 543–553.

[18] Hansen, A. H., Childress, D. S., and Knox, E. H., 2000, "Prosthetic Foot Roll-over Shapes with Implications for Alignment of Trans-tibial Prostheses," Prosthetics and Orthotics International, **24**(3), pp. 205–215.

[19] Hansen, A. H., Meier, M. R., Sam, M., Childress, D. S., and Edwards, M. L., 2003, "Alignment of Trans-Tibial Prostheses Based on Roll-over Shape Principles," Prosthetics and Orthotics International, **27**(2), pp. 89–99.

[20] Sam, M., et al., 2004, "The 'Shape&Roll' Prosthetic Foot: I. Design and Development of Appropriate Technology for Low-income Countries," Medicine, Conflict, and Survival, **20**(4): pp. 294-306.

[21] Meier, M. R., Sam, M., Hansen A. H., and Childress, D.S., 2004, "The 'Shape&Roll' Prosthetic Foot: II. Field Testing in El Salvador." Medicine, Conflict, and Survival **20**(4): pp. 307-325.

[22] Sam, M., Hansen, A. H., and Childress, D. S., 2004, "Characterisation of Prosthetic Feet Used in Low-Income Countries," Prosthetics and Orthotics International, **28**(2), pp. 132–140.

[23] Kapp, S., and Cummings, D., 1992, *Atlas of Limb Prosthetics: Surgical, Prosthetic, and Rehabilitation Principles*, 2nd ed., Bowker, H. K., and Michael, J. W., eds., American Academy of Orthopedic Surgeons, Rosemont, IL, Chap. 18b.

[24] Össur Americas, "Flex-Foot Assure Catalog page," from https://assets.ossur.com/library/29817/Flex-Foot Assure Catalog page.pdf

[25] Klodd, E., Hansen, A., Fatone, S., and Edwards, M., 2010, "Effects of Prosthetic Foot Forefoot Flexibility on Gait of Unilateral Transtibial Prosthesis Users," The Journal of Rehabilitation Research and Development, **47**(9), pp. 899-910.

[26] Olesnavage, K. M., and Winter, A. G., 2015, "Lower Leg Trajectory Error: A Novel Optimization Parameter for Designing Passive Prosthetic Feet," IEEE 2015 International Conference On Rehabilitation Robotics, Institute of Electrical and Electronics Engineers, pp. 271–276.

[27] San Tsung, B. Y., Zhang, M., Fan, Y. B., and Boone, D. A., 2003, "Quantitative Comparison of Plantar Foot Shapes under Different Weight-Bearing Conditions," Journal of Rehabilitation Research and Development, **40**(6), p. 517.

[28] Carlsöö, S., and Wetzenstein, H., 1968, "Change of Form of the Foot and the Foot Skeleton Upon Momentary Weight-Bearing," Acta Orthopaedica Scandinavica, **39**(1–3), pp. 413–423.

[29] Versluys, R., Beyl, P., Van Damme, M., Desomer, A., Van Ham, R., and Lefeber, D., 2009, "Prosthetic Feet: State-of-the-Art Review and the Importance of Mimicking Human Ankle–foot Biomechanics," Disability and Rehabilitation: Assistive Technology, **4**(2), pp. 65–75.

[30] Wezenberg, D., Cutti, A. G., Bruno, A., and Houdijk, H., 2014, "Differentiation between Solid-Ankle Cushioned Heel and Energy Storage and Return Prosthetic Foot Based on Step-to-Step Transition Cost," Journal of Rehabilitation Research and Development, **51**(10), pp. 1579–1590.

[31] Fogelberg, D. J., Allyn, K. J., Smersh, M., and Maitland, M. E., 2016, "What People Want in a Prosthetic Foot: A Focus Group Study," Journal of Prosthetics and Orthotics, **28**(4), pp. 145–151.

[32] Hafner, B. J., Morgan, S. J., Abrahamson, D. C., and Amtmann, D., 2016, "Characterizing Mobility from the Prosthetic Limb User's Perspective: Use of Focus Groups to Guide Development of the Prosthetic Limb Users Survey of Mobility," Prosthetics and Orthotics International, **40**(5), pp. 582–590.

[33] University of Dayton Design of Innovative Machines Laboratory, 2012, "Shape-Changing Spoiler," YouTube, from https://youtu.be/EwNuIGO_apA.

[34] Myszka, D. H., 2012, *Machines and Mechanisms: Applied Kinematic Analysis*, Prentice Hall, Boston, MA, Chap. 1.7.

[35] Murray, A. P., Schmiedeler, J. P., and Korte, B. M., 2008, "Kinematic Synthesis of Planar, Shape-Changing Rigid-Body Mechanisms," Journal of Mechanical Design, **130**(3), pp. 032302-1-10.

[36] Persinger, J. A., Schmiedeler, J. P., and Murray, A. P., 2009, "Synthesis of Planar Rigid-Body Mechanisms Approximating Shape-changes Defined by Closed Curves," Journal of Mechanical Design, **131**(7), p. 071006.

[37] Shamsudin, S. A., Murray, A. P., Myszka, D. H., and Schmiedeler, J. P., 2013, "Kinematic Synthesis of Planar, Shape-changing, Rigid-body Mechanisms for Design Profiles with Significant Differences in Arc Length," Mechanism and Machine Theory, **70**, pp. 425–440.

[38] Zhao, K., Schmiedeler, J. P., and Murray, A. P., 2012, "Design of Planar, Shape-Changing Rigid-Body Mechanisms for Morphing Aircraft Wings," Journal of Mechanisms and Robotics, **4**(4), p. 041007.

[39] Giaier, K. S., 2014, "Designing Shape-changing Mechanisms for Planar and Spatial Applications," M.S. thesis, Department of Mechanical & Aerospace Engineering, University of Dayton.

[40] Li, B., Murray, A. P., Myszka, D. H., and Subsol, G., 2016, "Synthesizing Planar Rigid-Body Chains for Morphometric Applications," ASME 2016 International Design Engineering Technical Conferences and Computers and Information in Engineering Conference, American Society of Mechanical Engineers, pp. V05BT07A036–V05BT07A036.

[41] Lee, Y.-C., and Wang, M.-J., 2015, "Taiwanese Adult Foot Shape Classification Using 3D Scanning Data," Ergonomics, **58**(3), pp. 513–523.

[42] Chong, A. K., Al-Baghdadi, J. A., and Milburn, P., 2015, "Human Plantar Pressure Image and Foot Shape Matching," Journal of Biosciences and Medicines, **3**(6), pp. 36–41.

[43] Kimura, M., Mochimaru, M., and Kanade, T., 2011, "3D Measurement of Feature Cross-Sections of Foot While Walking," Machine Vision and Applications, **22**(2), pp. 377–388.

[44] Luximon, A., Goonetilleke, R. S., and Zhang, M., 2005, "3D Foot Shape Generation from 2D Information," Ergonomics, **48**(6), pp. 625–641.

[45] Rifkin, J., 2009, "Joints for Prosthetic, Orthotic and/or Robotic Devices," U.S. Patent Application 20110015762A1.

[46] Yang, J., Abdel-Malek, K., and Potratz, J., 2005, "Design and Prototyping of an Active Hand Prosthetic Device," Industrial Robot: An International Journal, **32**(1), pp. 71–78.

[47] Liu, Y., Feng, F., and Gao, Y., 2014, "HIT Prosthetic Hand Based on Tendon-Driven Mechanism," Journal of Central South University, **21**(5), pp. 1778–1791.

[48] Rossi, C., Savino, S., Niola, V., and Troncone, S., 2015, "A Study of a Robotic Hand with Tendon Driven Fingers," Robotica, **33**(05), pp. 1034–1048.

[49] Ficanha, E. M., Rastgaar, M., and Kaufman, K. R., 2014, "A Two-Axis Cable-Driven Ankle-Foot Mechanism," Robotics and Biomimetics, **1**(1), p. 17.

[50] Collins, S. H., and Kuo, A. D., 2010, "Recycling Energy to Restore Impaired Ankle Function during Human Walking," PLoS ONE, **5**(2), p. e9307.

[51] Collins, S. H., Wiggin, M. B., and Sawicki, G. S., 2015, "Reducing the Energy Cost of Human Walking Using an Unpowered Exoskeleton," Nature, **522**(7555), pp. 212–215.

[52] Štrbac, M., and Popović, D. B., 2012, "Software Tool for the Prosthetic Foot Modeling and Stiffness Optimization," Computational and Mathematical Methods in Medicine, vol. 2012, pp. 1–8.

[53] Olesnavage, K. M., and Winter, A. G., 2017, "Passive Prosthetic Foot Shape and Size Optimization Using Lower Leg Trajectory Error," ASME 2017 International Design Engineering Technical Conferences and Computers and Information in Engineering Conference, American Society of Mechanical Engineers, pp. V05AT08A011.

[54] Olesnavage, K. M., and Winter, A. G., 2015, "Design and Qualitative Testing of a Prosthetic Foot With Rotational Ankle and Metatarsal Joints to Mimic Physiological Roll-over Shape," ASME 2015 International Design Engineering Technical Conferences and Computers and Information in Engineering Conference, American Society of Mechanical Engineers, pp. V05AT08A035–V05AT08A035.

[55] Winter, D. A., 2009, *Biomechanics and Motor Control of Human Movement*, 4th ed. John Wiley & Sons, Inc.

[56] Rahimi, A., and Mashak, A., 2013, "Review on Rubbers in Medicine: Natural, Silicone and Polyurethane Rubbers," Plastics, Rubber and Composites, **42**(6), pp. 223–230.

[57] Gore, A. I., and Spencer, J. P., 2004, "The Newborn Foot," American Family Physician, **69**(4), pp. 865–874.

Appendix

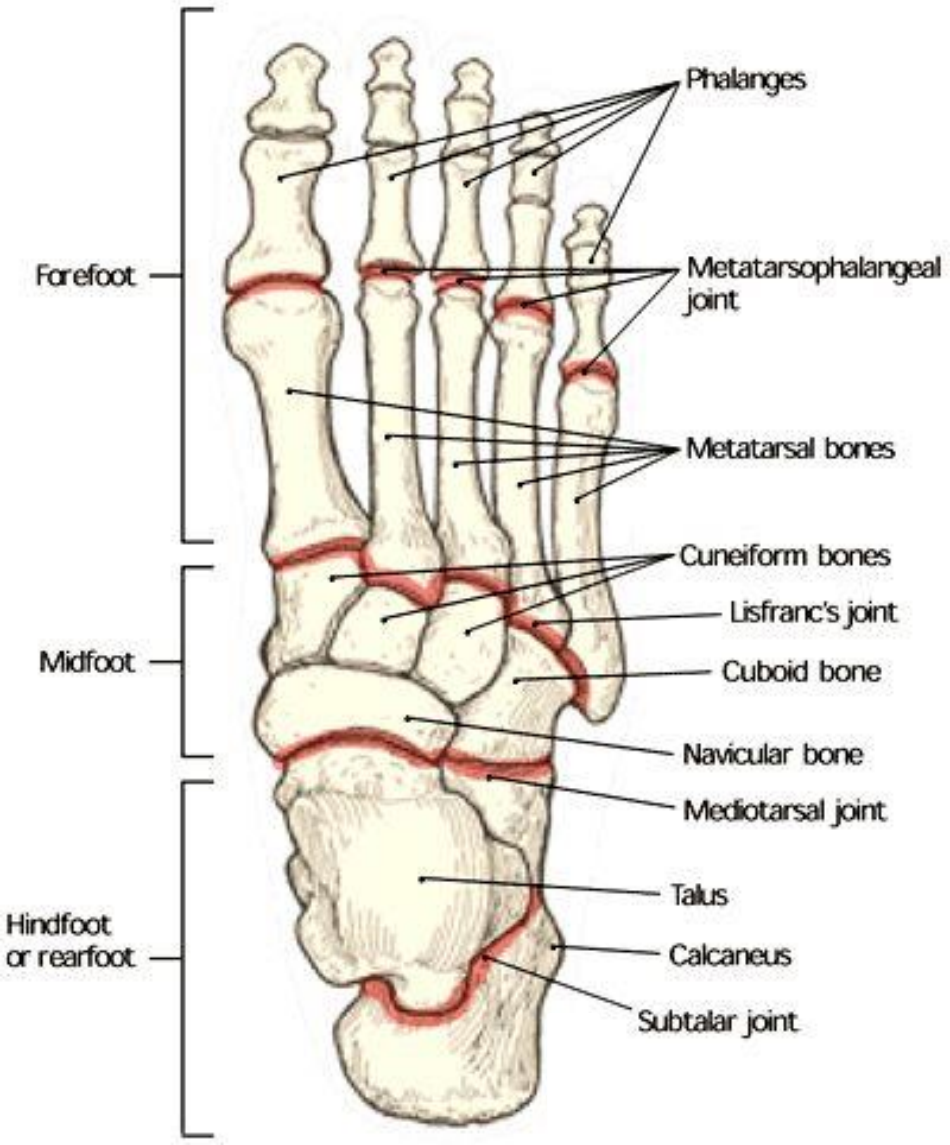

Figure A1. *Major bones and joints in the human foot. Image adapted from Ref. [57].*

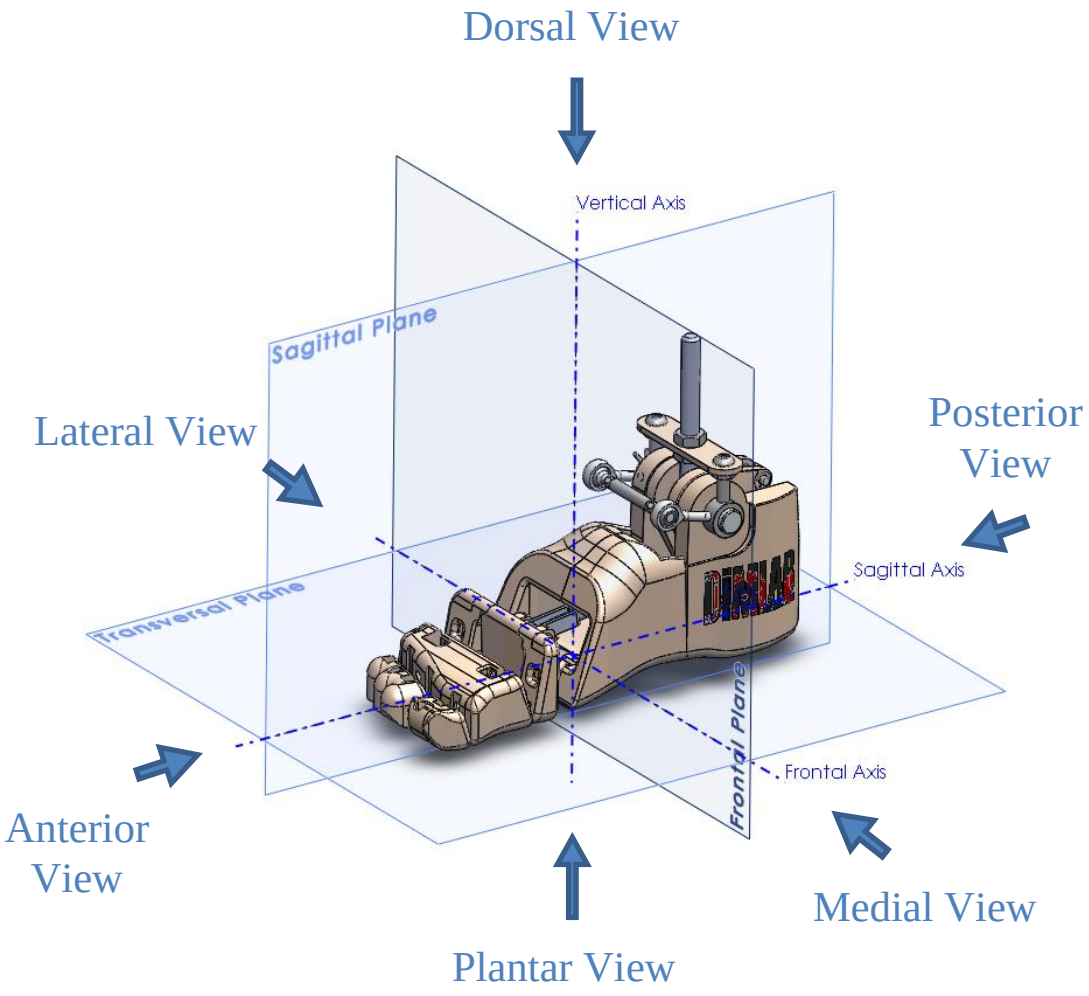

Figure A2. *Anatomical planes, axes, and views of the foot.*